The Plant Cell, Vol. 25: 4525–4543, November 2013, www.plantcell.org

Pollen Tube Growth Regulation by Free Anions Depends on the Interaction between the Anion Channel SLAH3 and Calcium-Dependent Protein Kinases CPK2 and CPK20[C][W]

Timo Gutermuth,[a,b] Roman Lassig,[d] Maria-Teresa Portes,[a] Tobias Maierhofer,[b] Tina Romeis,[d] Jan-Willem Borst,[c] Rainer Hedrich,[b] José A. Feijó,[a,e,f,1] and Kai R. Konrad[a,b]

[a] Gulbenkian Institute of Science, P-2780-156 Oeiras, Portugal
[b] Department of Botany I, Julius-Von-Sachs Institute for Biosciences, University of Wuerzburg, 97082 Wuerzburg, Germany
[c] Laboratory of Biochemistry and Microspectroscopy Centre, Wageningen University, 6708 Wageningen, The Netherlands
[d] Department of Plant Biochemistry, Dahlem Centre of Plant Sciences, Free University of Berlin, 14195 Berlin, Germany
[e] Faculty of Sciences, Department of Plant Biology, University of Lisbon, P-1749-016 Lisbon, Portugal
[f] Department of Cell Biology and Molecular Genetics, University of Maryland, College Park, Maryland 20742-5815

ORCID ID: 0000-0002-1100-5478 (J.A.F.).

Apical growth in pollen tubes (PTs) is associated with the presence of tip-focused ion gradients and fluxes, implying polar localization or regulation of the underlying transporters. The molecular identity and regulation of anion transporters in PTs is unknown. Here we report a negative gradient of cytosolic anion concentration focused on the tip, in negative correlation with the cytosolic Ca^{2+} concentration. We hypothesized that a possible link between these two ions is based on the presence of Ca^{2+}-dependent protein kinases (CPKs). We characterized anion channels and CPK transcripts in PTs and analyzed their localization. Yellow fluorescent protein (YFP) tagging of a homolog of *SLOW ANION CHANNEL-ASSOCIATED1* (SLAH3:YFP) was widespread along PTs, but, in accordance with the anion efflux, CPK2/CPK20/CPK17/CPK34:YFP fluorescence was strictly localized at the tip plasma membrane. Expression of SLAH3 with either CPK2 or CPK20 (but not CPK17/CPK34) in *Xenopus laevis* oocytes elicited S-type anion channel currents. Interaction of SLAH3 with CPK2/CPK20 (but not CPK17/CPK34) was confirmed by Förster-resonance energy transfer fluorescence lifetime microscopy in *Arabidopsis thaliana* mesophyll protoplasts and bimolecular fluorescence complementation in living PTs. Compared with wild-type PTs, *slah3-1* and *slah3-2* as well as *cpk2-1 cpk20-2* PTs had reduced anion currents. Double mutant *cpk2-1 cpk20-2* and *slah3-1* PTs had reduced extracellular anion fluxes at the tip. Our studies provide evidence for a Ca^{2+}-dependent CPK2/CPK20 regulation of the anion channel SLAH3 to regulate PT growth.

INTRODUCTION

Pollen tubes are formed by germination of pollen upon landing on the stigma of flowering plants. Their reproductive function is to carry the gametes through the pistil to the embryo sac in order to deliver the two sperm cells for double fertilization. Pollen tubes are specialized plant cells that grow very rapidly exclusively at the tip (Boavida et al., 2005; Feijó, 2010). They are also highly sensitized cells to various ion fluxes (Michard et al., 2009), making them natural cell biology models for ion signaling (Feijó et al., 2004; Konrad et al., 2011). In fact, a close regulation of ion dynamics, namely in terms of distinct patterns of extracellular fluxes and the formation of cytosolic ion gradients, is associated with pollen tube growth (Michard et al., 2009). Studies based on chemical and genetically encoded reporters showed that tip-focused cytosolic calcium ($[Ca^{2+}]_{cyt}$) and proton (H^+) gradients direct pollen tube growth (Pierson et al., 1994; Feijó et al., 1999; Michard et al., 2008). These cytosolic ion gradients are in line with the amplitude and direction of extracellular Ca^{2+} fluxes and H^+ fluxes and it is generally accepted that the cytosolic gradients are, to a great extent, a consequence of local plasma membrane ion fluxes (Michard et al., 2009; Hepler and Winship, 2010). Protons enter the pollen tube tip via a yet unknown transport system, but a pronounced H^+ efflux is maintained behind the subapical region (Feijó et al., 1999). This H^+-flux pattern is explained by and large by the active exclusion of H^+-ATPase(s) from the tip (Certal et al., 2008). The tip Ca^{2+} gradient decreases sharply from very high levels (at the micromolar level) near the inner surface of the plasma membrane at the tip, to basal (100 to 300 nM) levels (~20 μm) behind the tip (Holdaway-Clarke et al., 1997; Gilroy and Jones, 2000). This $[Ca^{2+}]_{cyt}$ gradient correlates well with growth speed, being most pronounced in rapidly elongating pollen tubes. Two glutamate receptor-like (GLR) genes, GLR3.7 and GLR1.2, were recently linked to Ca^{2+} transport and pollen tube growth (Michard et al., 2011).

A widespread feature of pollen tubes is the sustained growth oscillations when growing on artificial in vitro conditions (Feijó et al., 2001). Almost all physiological parameters of the cell oscillate, including cytoplasmic Ca^{2+} and H^+ concentrations and plasma membrane ion fluxes (Holdaway-Clarke et al., 1997; Feijó, 1999; Feijó et al., 2001). To the extent that all of these oscillations

[1] Address correspondence to jfeijo@umd.edu.
The author responsible for distribution of materials integral to the findings presented in this article in accordance with the policy described in the Instructions for Authors (www.plantcell.org) is: Kai R. Konrad (kai.konrad@botanik.uni-wuerzburg.de).
[C] Some figures in this article are displayed in color online but in black and white in the print edition.
[W] Online version contains Web-only data.
www.plantcell.org/cgi/doi/10.1105/tpc.113.118463

share approximately the same central period and comparable relative amplitudes, they seem to be coordinated by the same oscillator (Feijó et al., 1999, 2001; Moreno et al., 2007).

Anion fluxes, likely derived from chloride (Cl^-) activity, were also described in lily (*Lilium longiflorum*) and tobacco (*Nicotiana tabacum*), forming a closed loop of fluxes in the apical domain, with pronounced oscillatory efflux at the tip and nonoscillatory anion influx behind the tip (Zonia et al., 2001, 2002). Subsequent studies by patch clamp of pollen protoplasts suggest that these fluxes are derived from $[Ca^{2+}]_{cyt}$ activated anion channel activity in lily (Tavares et al., 2011a). Thus far, however, the molecular nature and mechanisms of the pollen tube anion transporters and regulators are largely unknown. Oscillations in cytoplasmic Ca^{2+} levels and plasma membrane anion channel activity are also a feature of guard cell action and stomatal movement (Allen et al., 2000, 2001; Konrad and Hedrich, 2008). In this system, there is more knowledge of the ion transporters and regulator repertoire, as recently reviewed by Roelfsema et al. (2012), and S- and R-type anion channels were recently associated with specific genes (Keller et al., 1989; Schroeder and Hagiwara, 1989; Negi et al., 2008; Vahisalu et al., 2008; Meyer et al., 2010). Of relevance, *SLOW ANION CHANNEL-ASSOCIATED1* (SLAC1) and its homolog SLAH3 were associated with the S-type anion currents. Both S-type anion channels are activated by phosphorylation through distinct calcium-dependent protein kinases (CPKs), namely CPK21, CPK23, CPK6, and CPK3 (Geiger et al., 2010, 2011; Brandt et al., 2012; Scherzer et al., 2012). Interestingly, CPKs harbor different Ca^{2+} affinities, indicating that CPK23 and CPK6 are active at resting $[Ca^{2+}]_{cyt}$, whereas CPK21 and CPK3 require an increase in $[Ca^{2+}]_{cyt}$ to phosphorylate the anion channels (Geiger et al., 2010).

In pollen tubes, anion effluxes at the tip match growth oscillations in both frequency and phase, pointing to a close link to growth regulation. Inhibition of anion fluxes in pollen tubes or grains via inhibitors results in growth arrest or retains pollen germination, respectively; furthermore, pharmacological and osmotic manipulations suggest that anion effluxes have a crucial role in water homeostasis (Zonia et al., 2002; Breygina et al., 2010). Patch-clamp studies revealed three different anion channel conductances in pollen grains and tube protoplasts (Tavares et al., 2011a).

The CPK family comprises 34 members with functional redundancy (Hrabak et al., 2003) and Plant Membrane Protein Database analysis (http://aramemnon.botanik.uni-koeln.de/) revealed that almost one-third of the CPK family proteins are specifically expressed in pollen (Pina et al., 2005). Mutations of CPK17 and CPK34 were found to have phenotypes in *Arabidopsis thaliana* pollen tube growth (Myers et al. 2009) and CPK11 and CPK24 were recently shown to modulate the activity of the pollen tube's inward rectifying Shaker potassium channel (SPIK) (Zhao et al., 2013); however, other than these CPKs, the physiological role of pollen-specific CPKs is largely unknown (Konrad et al., 2011).

Here we tested the hypothesis that the anion extracellular fluxes and currents previously described are able to form a specific cytosolic gradient, with a potential role in growth regulation. Furthermore, we hypothesized that the S-type anion channel SLAH3 is one of the molecular components that regulates these currents. Using a combination of methods, we substantiated these hypotheses and further identified SLAH3 in complexes at the pollen tube tip with the Ca^{2+}-dependent protein kinases CPK2 and CPK20. This interaction was confirmed by current measurements in *X. laevis* oocytes, Förster-resonance energy transfer fluorescence lifetime microscopy (FRET-FLIM) in *Arabidopsis* mesophyll protoplasts, and bimolecular fluorescent complementation (BiFC) on live pollen tubes. Our findings support a role for CPK2/CPK20-mediated activation of SLAH3 in delimited Ca^{2+} and cytosolic anion gradients at the pollen tube tip, and provide a framework for ion signaling integration in this apical growing cell.

RESULTS

Growing Pollen Tubes Possess a Cytosolic Anion Concentration Gradient and Apical Anion Oscillations

In lily and tobacco, pollen tube growth is associated with quasi-steady or oscillatory anion effluxes at the tip, always correlated with growth rate; furthermore, the large efflux at the tip is accompanied by a steady, nonoscillatory anion influx behind the tip (>10 to 15 μm; Zonia et al., 2002). From the chemo-osmotic point of view, the rapid anion flux variations associated with the pollen tube tip favor a passive anion channel–driven ion translocation mechanism rather than a carrier-driven transport. To investigate the physiological role of Cl^- in pollen tube growth, we measured *N. tabacum* pollen tube diameters under various extracellular anion concentrations. The pollen tube diameter increased during an increase in extracellular Cl^- concentration from 0.4 to 1, 10, 25, and finally 50 mM Cl^-. In seven time-series experiments of the same Cl^- concentration series, the tube diameters were 10.2 ± 1.3 μm, 10.3 ± 1.5 μm, 10.8 ± 1.1 μm, 11.2 ± 1.0 μm, and 12.0 ± 0.9 μm, respectively. The diameter increased by 18% in 50 mM Cl^- compared with the 0.4 mM control medium. We thus hypothesized that the extracellular anion concentration changes feedback on cytosolic anion homeostasis. To test this hypothesis, we performed live-cell imaging experiments on biolistically transformed *N. tabacum* pollen tubes. We expressed the genetic anion-sensitive probe *Chloride-Sensor* to monitor changes in anion level (Markova et al., 2008). This cyan fluorescent protein (CFP)-yellow fluorescent protein (YFP) based FRET sensor for anions has a relatively high anion sensitivity (K_{app} ~30 mM) in contrast with previous genetically encoded anion sensors (Lorenzen et al., 2004). *Chloride-Sensor*–expressing tobacco pollen tubes were exposed to an increase in extracellular chloride concentration. False color–coded ratio images of such a pollen tube recording are exemplified in the time series displayed in Figure 1A (see Supplemental Movie 1 online). To visualize the dynamic anion distribution of the whole time-series experiment, we generated a kymograph of the pollen tube ratio signal (Figure 1B). A kymograph is an intuitive way to present ratio intensity dynamics in one dimension over time. Standard growth conditions with 0.4 mM Cl^- in the medium revealed a cytosolic anion gradient. High ratio values, symbolizing high anion concentrations, were apparent in the region 20 to 50 μm behind the tip. In contrast, the tip and subapical region (0 to 10 μm behind the tip) as well as the base of the tube (≥50 μm behind the tip) revealed a relatively low ratio value (Figures 1A and 1B). This anion distribution pattern was maintained during an increase in extracellular chloride concentration (1, 10, 25, and 50 mM Cl^-), but the overall ratio intensity signal increased in stepwise fashion after each gradual concentration increase (Figures 1A

and 1B). The application of 25 μM 5-nitro-2-(3-phenylpropylamino) benzoic acid (NPPB), an efficient anion channel blocker (Schroeder et al., 1993), resulted in a dramatic decrease in ratio signal, growth arrest (Figures 1A and 1B), and, eventually, pollen tube death. Interestingly, pronounced growth oscillations were observed after the application of ≥10 mM chloride, symbolized by the alternating modification of the kymograph slope (Figure 1B), as indicated by the arrows in Figure 1C. A detailed analysis of pollen tube growth velocity (red) and apical cytosolic anion concentration ($[anion]_{cyt}$, black) in Figure 1D demonstrates an apparent correlation in terms of period, and that these periods are in counter-phase. A burst of growth was always accompanied by a decrease of the tip-focused ratio value, equivalent to a decrease in anion concentration in the pollen tube tip (Figure 1D). This observation is in line with vibrating probe studies using anion-selective extracellular electrodes, demonstrating anion effluxes at the tip, which is most pronounced when the outburst of a growth cycle begins (Zonia et al., 2002). Interestingly, the period of the simultaneous growth and apical anion oscillations increased with increasing extracellular Cl^- concentrations. A possible interference of the *Chloride Sensor* ratio signal through the well-described pH gradient in growing pollen tubes was evaluated using the ratiometric cytosolic pH-sensor pHluorin (Miesenböck et al., 1998). Again, we biolistically transformed tobacco pollen and performed cytosolic pH measurements during an increase in extracellular Cl^- concentration, using an experimental design similar to the one described for Figure 1. If a pronounced pH effect within the *Chloride Sensor* ratio signal exists, one would expect a similar cytosolic ratio signal using the two probes. Interestingly, an elevation in extracellular chloride concentration increased the apical pH gradient at the tip (see Supplemental Figure 1 online); however, the relative anion concentration in the extreme tip does not vary in such a fashion (Figure 1). In addition, a change in cytosolic pH could not be detected in the zone behind the subapical region (~20 to 40 μm behind the tip) (see Supplemental Figure 1 online), where a pronounced increase in the *Chloride Sensor* ratio value occurs (Figure 1). A comparison of the ratio signal of both probes thus illustrated their fundamental differences along growing pollen tubes during an increase in the extracellular chloride concentration and point to negligible crosstalk (Figure 1; see Supplemental Figure 1 online) within our experimental design. Interestingly, the apical pH gradient started to oscillate when we increased the extracellular chloride concentration (see Supplemental Figure 1 online).

Correlation between a Cytosolic Anion Concentration Gradient and Ca^{2+} Homeostasis at the Tip

On in vitro growing conditions (especially in tobacco and lily), it is well established that pollen tubes tend to display oscillations in growth rate, which are associated with changes in tip-localized $[Ca^{2+}]_{cyt}$ changes in various species (Heslop-Harrison et al., 1985; Holdaway-Clarke et al., 1997; Camacho et al., 2000; Lazzaro et al., 2005; Michard et al., 2008). A set of CPKs was recently demonstrated to regulate anion channel activity in guard cells (Geiger et al., 2009b, 2010, 2011; Brandt et al., 2012; Scherzer et al., 2012). To test whether a relationship exists between anion and Ca^{2+} homeostasis at the pollen tube tip, we expressed the $[Ca^{2+}]_{cyt}$ reporter Yellow-Cameleon YC3.6 (Nagai et al., 2004). Transiently transformed tobacco pollen grains were grown in medium containing 0.4 mM chloride and $[Ca^{2+}]_{cyt}$ was monitored upon the application of 10 mM chloride, as in Figure 1. The false color–coded kymograph of time-lapse images of a representative pollen tube expressing YC3.6 time is presented in Figure 2A. Simultaneous analysis of the tip-focused $[Ca^{2+}]_{cyt}$ gradient and growth rate (Figure 2B) demonstrates a weakly oscillating tip-focused $[Ca^{2+}]_{cyt}$ gradient under standard growth conditions (Figure 2). Upon application of 10 mM chloride, however, pronounced growth alterations were recorded and tip-focused $[Ca^{2+}]_{cyt}$ started to oscillate robustly. High $[Ca^{2+}]_{cyt}$ at the tip correlated with increased growth velocity, which corresponded with a reduction in cytosolic anion concentration at the tip (Figure 1), indicating a temporal coupling of anion and Ca^{2+} homeostasis. In support of this observation, switching back from 10 mM to 0.4 mM extracellular chloride (wash-out) resulted in a dampening of the $[Ca^{2+}]_{cyt}$ and growth velocity oscillations. Application of 5 μM NPPB, however, abolished the tip-focused $[Ca^{2+}]_{cyt}$ gradient and reduced growth velocity (Figure 2; see Supplemental Movie 2 online).

Identification and Subcellular Localization of Pollen Tube Anion Channels

To identify anion channels expressed in pollen tubes, quantitative RT-PCR (qRT-PCR) was performed with cDNA ($n = 5$) from in vitro grown *Arabidopsis* pollen tubes. The transcript numbers of SLAC/SLAH-type and ALUMINUM-ACTIVATED MALATE TRANSPORTER/QUICKLY ACTIVATING ANION CHANNEL (ALMT/QUAC)-type anion channel proteins (known or postulated) were normalized to 10,000 actin2/8 transcripts. Relative transcript numbers of SLAH3 and ALMT12 were 919.8 ± 108.8 and 401.8 ± 122.4, respectively (Figure 3A). Transcripts of SLAC1 were at the detection level (10.5 ± 1.2 relative transcripts), whereas other members of the SLAC/SLAH family (namely SLAH1, SLAH2, and SLAH4) appeared not to be expressed in pollen tubes (Figure 3A). Both SLAH3 and ALMT12 were thus considered as pollen anion channels (Figure 3A). Employing a SLAH3 promotor–β-glucuronidase (GUS) line, SLAH3 expression was confirmed in pollen grains and pollen tubes within the pistil of *Arabidopsis* (Figure 3B). Because SLAH3 was already identified as a target of CPK action in guard cells, we decided to focus on the effect of SLAH3 on pollen tube performance. First we biolistically transformed *N. tabacum* pollen tubes and determined the subcellular localization of SLAH3. The fusion protein of YFP:SLAH3 (see Supplemental Figure 2 online) and SLAH3:YFP (Figure 3D) showed a uniform plasma membrane fluorescence with a slight tendency to decrease toward the apex. In contrast with the plasma membrane anion channel, soluble YFP (Venus) could be detected throughout the cytosol (Figure 3C).

Subcellular Localization of Pollen Tube CPKs

The S-type anion channel SLAH3 is expressed in guard cells and mesophyll cells and its activation depends on *trans*-phosphorylation of CPK21/CPK23 (Geiger et al., 2011). We hypothesized that in the context of tip growth, pollen tube expressed CPKs could also interact with SLAH3. On the basis of results of a database analysis (http://aramemnon.botanik.uni-koeln.de/) and transcriptomic data from Pina et al. (2005), we cloned the 12 pollen-expressed CPKs

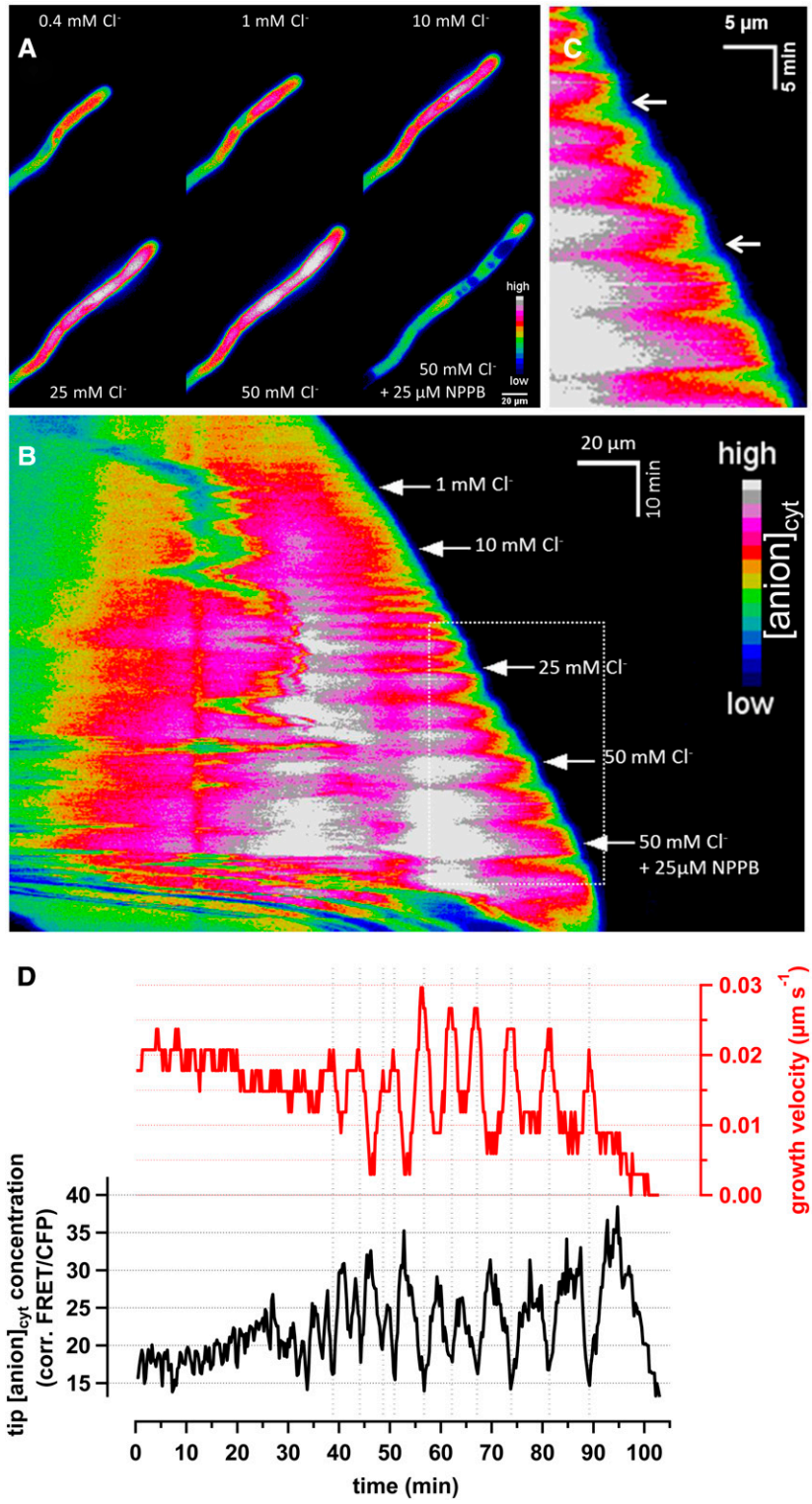

Figure 1. Spectroscopic Detection of a Cytosolic Chloride Gradient in Pollen Tubes.

Transient (biolistic) expression of *Cl⁻-Sensor* in *N. tabacum* pollen tubes.
(A) Time-lapse fluorescence false color–coded ratio images of representative pollen tubes subjected to increasing concentrations of chloride (1, 10, 25, and 50 mM Cl^-, as displayed in the graph). The anion channel inhibitor NPPB was applied in the end of the sequence (see Supplemental Movie 1 online).

and transiently expressed them as YFP fusion proteins in *N. tabacum* pollen tubes. The CPK family comprises 34 members that can be divided into four subgroups (Hrabak et al., 2003). The majority of CPK family members harbor a putative N-terminal myristoylation and/or palmitoylation site, suggesting that they are membrane- or membrane-associated target proteins (Cheng et al., 2002). CPK4, CPK11, and CPK26 are relatively closely related proteins from subgroup I. These kinases are predicted to lack a myristoylation site (Cheng et al., 2002) and they indeed revealed a cytoplasmic fluorescence signal when fused to a YFP protein (Figure 4, top left). CPK14, CPK16, CPK24, and CPK32 from subgroups III and IV are predicted to be myristoylated and appeared to have a dual-subcellular localization. A minor plasma membrane fluorescence signal was detected, which was absent from the tip. However, the main fluorescent signal of CPK24 was visible in the vegetative nucleus (Figure 4, top right) and that of CPK14, CPK16, and CPK32 (Figure 4, bottom left) at the membrane of the generative cell. A more diffuse plasma membrane fluorescence of CPK6:YFP was detected in the base of the pollen tube with an increasing intensity toward the grain but it was absent from the membrane on the first 50 to 60 μm (Figure 4, second row, on right). Closely related CPK2 and CPK20, from subgroup I, are specifically expressed in pollen tubes and root hairs (M. Böhmer and T. Romeis, unpublished data). CPK2:YFP and CPK20:YFP revealed a plasma membrane fluorescence signal exclusively at the growing pollen tube tip (Figure 4, mid right). Tissue-specific GUS activity of transgenic *Arabidopsis* plants carrying *ProCPK2::GUS* or *ProCPK20::GUS* showed strong promoter activity in pollen (see Supplemental Figure 3 and Supplemental Table 1 online) and a tip-localized plasma membrane CPK2:YFP signal was confirmed in transgenic *Arabidopsis* plants carrying *ProLeLAT52::CPK2:YFP* (see Supplemental Figure 4 and Supplemental Table 1 online). Double loss-of-function mutants of the similar (93% amino acid identity) CPK17 and CPK34 are impaired in pollen tube growth and subsequently in fertilization (Myers et al., 2009). Both CPK17 and CPK34 are localized to the plasma membrane of the pollen tube tip (Figure 4, bottom right), but their physiological target proteins are not known. The subcellular localization of CPK2, CK20, CPK17, and CPK34 at the tip is in line with our hypotheses of CPK-induced anion channel activation. To test whether posttranscriptional modifications at the N-terminus are important for unique plasma membrane targeting of the latter CPKs, we generated point mutation constructs eliminating myristoylation and/or palmitoylation sites of CPK34 and CPK2. Eliminating either myristoylation or palmitoylation resulted in a cytoplasmic localization of both CPK proteins (see Supplemental Figure 5 online). An N-terminal YFP fusion of CPK34 and CPK2 prevented correct plasma membrane targeting as well, and gave rise to cytosolic fluorescence in pollen tubes expressing YFP:CPK34 or YFP:CPK2 (see Supplemental Figure 5 online). These results strongly indicate the necessity of posttranslational modification for the distinct subcellular localization patterns of membrane-associated pollen CPKs presented in Figure 4.

Protein–Protein Interaction between CPK2/20 and SLAH3

Next we hypothesized that pollen tube CPKs phosphorylate SLAH3 in a calcium-dependent fashion, similar to previous studies of the guard cell anion channels SLAH3 and SLAC1, which are activated via CPK21/CPK23 phosphorylation when coexpressed (Geiger et al., 2009, 2010, 2011). To identify interacting partners for SLAH3 among the putative CPK candidates localized to the pollen tube tip, we performed FRET-FLIM. Therefore, CPK17 and CPK34 as well as CPK2 and CPK20 with a C-terminal mTurquoise (CFP) fusion were either expressed alone or coexpressed with SLAH3:YFP in *Arabidopsis* mesophyll protoplasts. The CFP (donor) fluorescence lifetime was recorded under both conditions. Expression of CPK17 and CPK34 fused to CFP alone resulted in an average fluorescence lifetime of 3.159 ± 0.009 ns (n = 41) and 3.142 ± 0.006 ns (n = 38), respectively (Figure 5A, open bars). No significant reduction of the average fluorescence lifetime was detectable when CPK17:CFP or CPK34:CFP were coexpressed with SLAH3:YFP (Figure 5A, filled bars). The average fluorescence lifetimes of CPK2:CFP (n = 37) and CPK20:CFP (n = 37) alone were 3.130 ± 0.009 ns and 3.133 ± 0.005 ns, respectively, and were thus comparable with the average lifetimes of CPK17:CFP and CPK34:CFP alone. However, the average fluorescence lifetime was significantly reduced to 3.070 ± 0.012 ns (n = 35) and 3.081 ± 0.010 ns (n = 37), respectively, when CPK2:CFP and CPK20:CFP were coexpressed with SLAH3:YFP (Figure 5A). These results indicated a specific interaction of CPK2 ($P \leq 0.0002$) and CPK20 ($P \leq 0.0001$), but not CPK17 and CPK34, with the anion channel SLAH3. The average lifetime of CFP alone and a CFP:YFP fusion (2 amino acid linker) were compared as an additional control and gave rise to a strong reduction of the fluorescence lifetime from 3.172 ± 0.007 ns (n = 15) to 2.410 ± 0.035 ns (n = 16) in CFP:YFP expressing cells. A fluorescence lifetime reduction of 60.51 ps in CPK2 and 51.86 ps in CPK20 coexpressed with SLAH3 was much less than the decrease in the CFP:YFP fusion protein (762 ns), most likely because of the transient nature of the interaction between CPKs and their target proteins.

YFP BiFC was also used to test the association between SLAH3 and the different CPKs. Results and controls are shown in Supplemental Figure 6 online. However, in control experiments, a fluorescence complementation could be detected with

Figure 1. (continued).

(B) A kymograph of the same time-series experiments is displayed in the same false colored code. The *x*-axis and *y*-axis represent the distance and time, respectively.

(C) Magnification of the dotted rectangular selection in **(B).** Note the especially well-defined oscillations on growth and Cl^- concentration upon addition of 25 mM Cl^- (top arrow) and 50 mM Cl^- (bottom arrow).

(D) Simultaneous analysis of growth velocity (red) and cytosolic Cl^- concentrations in the apical 5 μm (black). Data are from the time series presented in **(A) to (C)**, and are considered to be representative (n = 8). Of special relevance, apical chloride concentration decreases when pollen tube growth accelerates, in an almost perfect counter-phase/negative correlation.

[See online article for color version of this figure.]

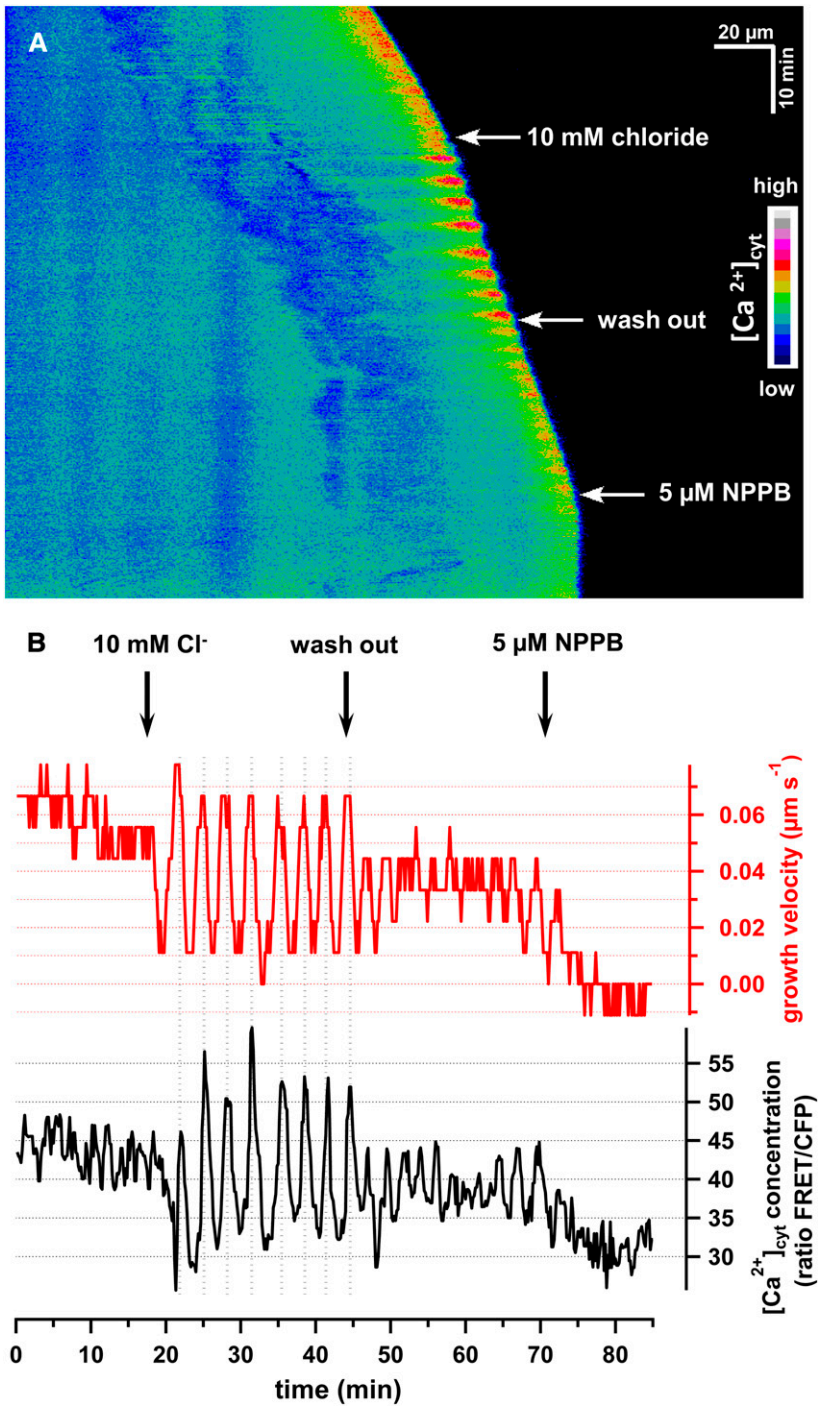

Figure 2. Extracellular Chloride Modifies the Cytosolic Tip-Focused Ca^{2+} Gradient in Pollen Tubes.

Cytosolic Ca^{2+} concentrations were detected by means of ratiometric measurements of biolistically transformed *N. tabacum* pollen tubes with the genetically encoded Ca^{2+} indicator YC3.6.

(A) False color–coded kymograph of a representative experiment of a growing pollen tube upon application of 10 mM chloride and 5 µM NPPB (see Supplemental Movie 2 online).

(B) Simultaneous analysis of tip-localized $[Ca^{2+}_{free}]_{cyt}$ and growth velocity of the experiment presented in **(A)**.

[See online article for color version of this figure.]

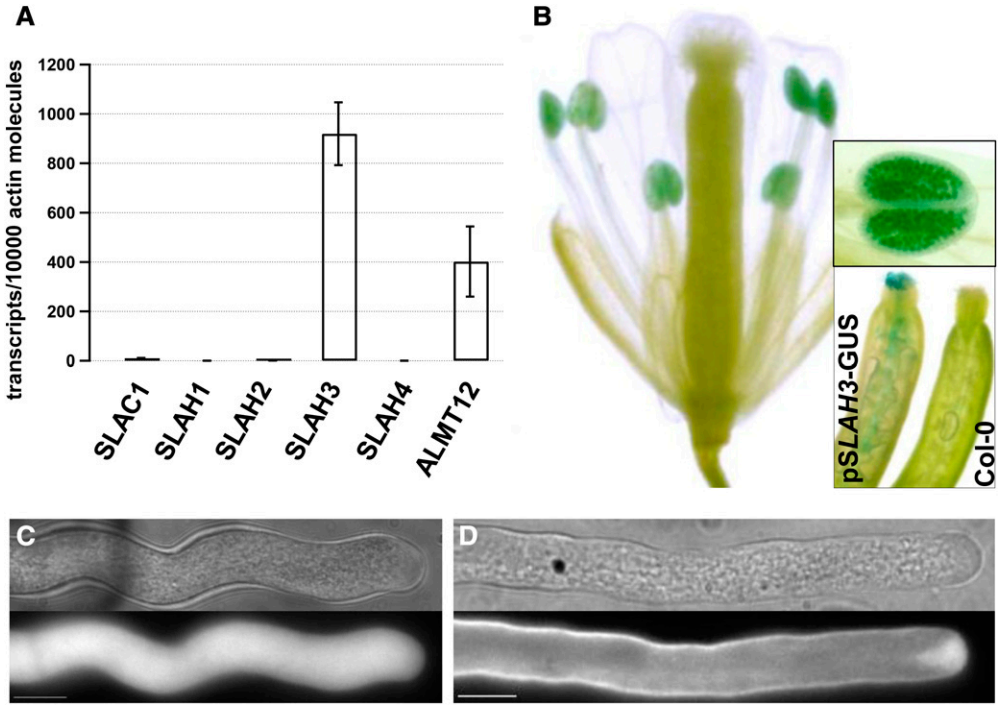

Figure 3. Identification and Subcellular Localization of the Anion Channel SLAH3 in Pollen Tubes.

(A) qRT-PCR analysis of anion channels in pollen tubes. Relative transcript numbers are presented for members of the SLAC/SLAH anion channel family and At ALMT12. RNA extraction and cDNA synthesis were performed on in vitro grown *A. thaliana* (ecotype Col-0) pollen tubes after 5 h of growth (n = 5). Bar indicates SE.

(B) SLAH3 promotor-GUS (ProSLAH3::GUS) gene expression in pollen of an *A. thaliana* flower. A magnification of an anther is presented in the top inlay. A comparison of a pollinated pistil of ProSLAH3::GUS (left) and wild-type Col-0 plant (right) is presented in the bottom right inlay.

(C) and (D) Biolistic transformation of *N. tabacum* pollen with SLAH3:YFP from *Arabidopsis* demonstrated the uniform plasma membrane localization of the anion channel **(D)** in contrast with soluble YFP **(C)**. Bar = 10 μm.

[See online article for color version of this figure.]

a coexpression of the C-terminal half of a YFP (YC) and the N-terminal half of the YFP (YN) alone or CPK11:YN + YC in the cytoplasm, CPK34:YN + YC at the membrane of the apex, and CPK21:YN + YC, SLAH3:YC + YN and CPK34:YN + SLAH3 uniformly at the plasma membrane (see Supplemental Figure 6 online). When BiFC constructs of YC:SLAH3 and CPK2:YN were coexpressed, it was difficult to find and image intact pollen tubes, because the majority collapsed and died. Interestingly, we detected a plasma membrane fluorescence complementation exclusively at the apex (see Supplemental Figure 6 online), pointing to a specific SLAH3/CPK2 complex forming only at the pollen tube tip. In combination with the FRET-FLIM results, these data suggest that SLAH3 and CPK2 interact. However, the pleiotropic localization responses observed for the different controls, most likely because of a general overexpression of the proteins, would advise for caution for direct conclusions from the BiFC data.

CPK2/CPK20-Mediated Activation of SLAH3 Currents in *X. laevis* Oocytes

To further detail the interaction between SLAH3 and tip-localized pollen-specific CPKs in relation to anion channel function, we took advantage of the two-electrode voltage clamp (TEVC) technique. We injected the cRNA of SLAH3 fused to the C-terminal half of YFP together with a variety of elongation factor (EF)-hand truncated (ΔEF) CPK versions (Geiger et al., 2011; Scherzer et al., 2012). CPK34, CPK17, CPK2, and CPK20 were fused to the N-terminal half of YFP in *X. laevis* oocytes to analyze ion currents and BiFC. In this type of experiment, BiFC conclusions are directly verifiable by the induction of currents. EF hand-truncated CPK versions were used because their kinase activity is independent of oocyte cytosolic Ca^{2+} variations. To resolve anion currents, voltage-clamped oocytes were exposed to a depolarization voltage pulse of 0 mV to allow channel activation, followed by 20-s voltage pulses ranging from +40 to −180 mV in 20-mV decrements. These voltage steps were followed by a 3-s voltage pulse to −120 mV. S-type anion channel activity is characterized by slow deactivating currents upon voltage steps from depolarized to hyperpolarized membrane potentials, whereas instantaneous or slowly activating currents are recorded in the depolarized voltage range. The expression of SLAH3:YC alone (as a negative control) or coexpression of SLAH3:YC with CPK17:YN or CPK34:YN did not elicit macroscopic anion currents (Figure 6A). However, coexpression of CPK2:YN or CPK20:YN with SLAH3:YC resulted in instantaneous

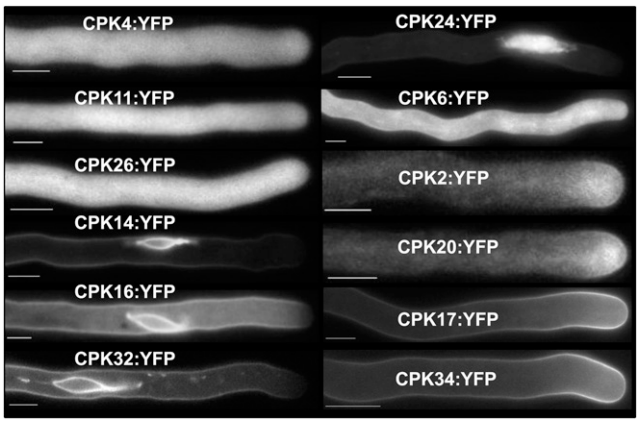

Figure 4. Subcellular Localization of All Pollen-Expressed CPKs.

Spectroscopic analysis of C-terminal YFP fusion proteins of pollen-expressed CPKs after transient expression in *N. tabacum* pollen tubes. Images are taken from in vitro grown pollen tubes 5 to 8 h after transformation. Representative fluorescence images are presented from ≥3 independent experiments with numerous pollen tubes recorded. The protein family members are indicated in the figure. Note the plasma membrane localization of CPK2, CPK20, CPK17, and CPK34 at the pollen tube tip. Bar = 10 μm.

currents ($P \leq 0.0001$) with typical time-dependent S-type anion channel deactivation kinetics (Figure 6A). CPK21, which is known to activate SLAH3 (Geiger et al., 2011), was coexpressed as a positive control and gave rise to macroscopic currents ($P \leq 0.0001$) comparable to those with CPK2 (Figure 6A). In line with a phosphorylation-dependent anion channel activation, point mutation versions of CPK2 ($CPK2_{D310A}$) and CPK20 ($CPK20_{D258A}$), rendering the kinase inactive, did not result in macroscopic SLAH3 currents. Mean steady state SLAH3 currents at −100 mV are presented upon coexpression with the CPKs as indicated in Figure 6B and revealed −11.3 ± 0.8 μA with CPK21 ($n = 8$), −9.90 ± 2.3 μA with CPK2 ($n = 11$), and −6.7 ± 1.6 μA with CPK20 ($n = 11$). For SLAH3:YC alone ($n = 10$), coexpression of the anion channel with CPK17 ΔEF:YN ($n = 8$), CPK34 ΔEF:YN ($n = 6$), $CPK2_{D310A}$ ΔEF:YN ($n = 4$), or $CPK20_{D258A}$ ΔEF:YN ($n = 4$) did not elicit macroscopic currents (Figure 6B). As expected, oocytes expressing SLAH3:YC alone exhibited no yellow fluorescence signal upon spectroscopic analysis (Figure 6C). Coexpression of SLAH3:YC with CPK17 ΔEF:YN or CPK34 ΔEF:YN resulted in weak YFP fluorescence, whereas CPK21 ΔEF:YN, CPK2 ΔEF:YN, CPK20 ΔEF:YN, $CPK2_{D310A}$ ΔEF:YN, and $CPK20_{D258A}$ ΔEF:YN showed a bright membrane BiFC signal, indicating a physical interaction between SLAH3 and CPK2, CPK20, and CPK21 (Figure 6C).

Anion Currents and Fluxes Are Reduced in *slah3-1, slah3-2,* and *cpk2-1 cpk20-2* Double Mutant Pollen Tubes

Double-barreled electrodes were used to impale growing *Arabidopsis* pollen tubes on a semi-solid medium to characterize anion currents using the TEVC technique. Wild-type and mutant pollen grains were germinated in parallel by dotting freshly harvested flowers on semi-solid medium (medium composition is indicated in the figure legends and in the Methods). To resolve pollen tube anion currents, a potassium-free medium was used to exclude typical time-dependent hyperpolarization activating K^+ currents (Fan et al., 2001; Mouline et al., 2002), which occur in the presence of ≥1 mM extracellular potassium (see Supplemental Figure 7 online). An increase in medium NO_3^- concentration from 1 to 5, 20, and 40 mM, while maintaining constant Ca^{2+} (20 mM) and nominal 0 mM K^+ concentration, resulted in a current amplitude increase in the negative and positive voltage range (Figure 7A). Negative or positive currents represent anion efflux from or influx into the cell, respectively. Increasing NO_3^- media concentrations resulted in a reversal potential shift toward more positive potentials. The

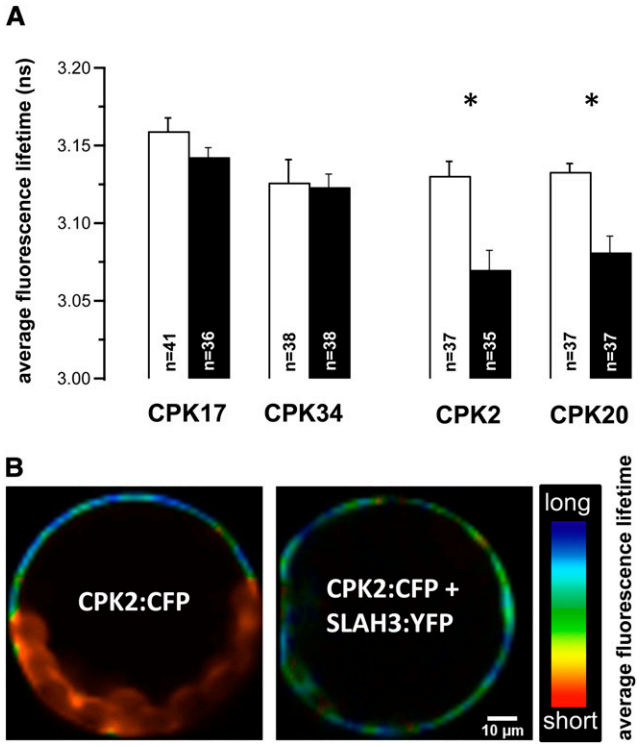

Figure 5. FRET-FLIM Analysis Identified SLAH3–CPK2/CPK20 Interaction.

Average fluorescence lifetime monitored in transiently transformed *A. thaliana* mesophyll protoplasts with a two-component fit.

(A) The average fluorescence lifetime of the donor CFP (mTurquoise) fluorescence is presented when CPKs fused to CFP were expressed alone (open bars) or coexpressed with SLAH3:YFP (filled bars). CPKs coexpressed with SLAH3 are indicated in the figure. The average fluorescence lifetime was compared between CFP and CFP:YFP (fusion protein with a 2 amino acid linker) as control. *$P \leq 0.0002$ (paired Student's *t* test).

(B) Pseudocolor-coded fluorescence lifetime images of an *Arabidopsis* mesophyll protoplast expressing CPK2:mTurquoise alone (left) or coexpressed with SLAH3:YFP (right). Note the presence of dark blue pixels at the plasma membrane in CPK2:mTurquoise-expressing protoplasts, whereas coexpression with SLAH3:YFP results in fewer dark blue but more cyan and green pixels (chloroplasts are characterized by very short lifetime distributions [red]).

[See online article for color version of this figure.]

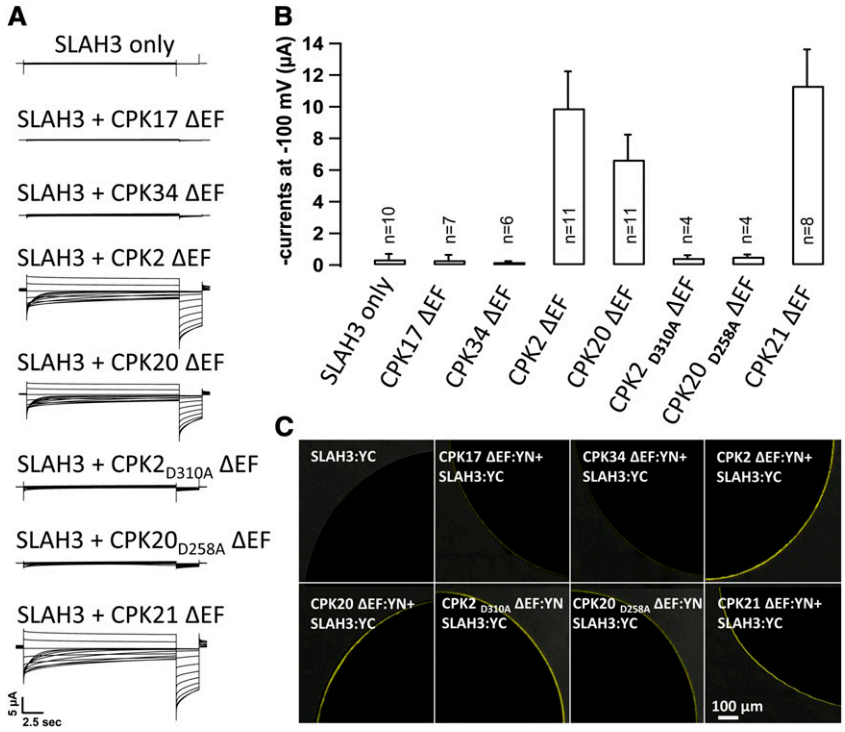

Figure 6. CPK2 and CPK20 Interact with and Activate SLAH3 in *X. Laevis* Oocytes.

(A) Whole-oocyte current recordings upon 20-s voltage pulses ranging from +40 to −180 mV in 20-mV decrements followed by a 3-s voltage pulse to −120 mV. After a preactivation voltage pulse of 0 mV, pronounced instantaneous anion currents could be measured with SLAH3:YC coexpressed with EF hand-truncated versions of CPK2, CPK20, and CPK21, but not with CPK17 or CPK34 fused to the N-terminal half of a YFP (YN). Coexpression of SLAH3:YC with point mutation mutants of CPK2 ($CPK2_{D310A}$) and CPK20 ($CPK20_{D258A}$) did not elicit macroscopic anion currents. Of special note, the slow channel deactivation is symbolized by the exponential decrease of negative currents at hyperpolarized membrane potentials. This reflects the weak voltage dependence of the depolarization-activated S-type anion channel SLAH3.

(B) The mean instantaneous currents of ≥4 measurements at −100 mV are presented for the coexpression of SLAH3:YC and EF hand-truncated versions of CPK17, CPK34, CPK2, CPK20, $CPK2_{D310A}$, $CPK20_{D258A}$, and CPK21 fused to YN. Coexpression of SLAH3:YC with CPK21:YN and only SLAH3:YC (control) were used as positive and negative controls, respectively. *P ≤ 0.0001. Bar indicates SD.

(C) Interaction studies by BiFC in the *X. laevis* oocytes analyzed in **(B)**. Note the YFP fluorescence complementation in oocytes coexpressing CPK2, CPK20, $CPK2_{D310A}$, $CPK20_{D258A}$, or CPK21 with SLAH3 but not in those coexpressing CPK17 or CPK34 with SLAH3.

[See online article for color version of this figure.]

reversal potentials at 5, 10, 20, and 40 mM medium NO_3^- concentration were −57.1 ± 3.2 mV, −48.1 ± 5.3 mV, −45.7 ± 3.0 mV, and −39.2 ± 8.9 mV, respectively. According to the Nernst equation, this indicates a cytosolic NO_3^- accumulation with increasing media anion concentration from 0.6 mM NO_3^- to 1.9 mM, 3.6 mM, and 8.9 mM, respectively (see Supplemental Table 2 online). In line with a 20 times higher NO_3^- to Cl^- permeability, and an extracellular NO_3^--dependent SLAH3 channel activation, we recorded higher anion currents in NO_3^- (n = 10) compared with Cl^- (n = 12) conditions (Figure 7A, inset). A plot of the steady state current/voltage (I/V) relation demonstrated an up to 1.7-fold increase in negative current for pollen grown in a 40 mM NO_3^--based versus 40 mM Cl^- -based medium (Figure 7A, inset). Because of the high variation in currents, only a significant difference in the voltage range from −200 to −160 mV was apparent. These S-type currents could be blocked by 10 and 50 µM of the anion channel blockers niflumic acid (NA) (n = 5) and NPPB (n = 6) by 78% and 70% at −200 mV, respectively (see Supplemental Figure 8 online). Currents were significantly blocked ($P \leq 0.05$) at all voltages applied except −40 and −20 mV for NPPB and at −40 mV for NA. These anion channel blockers are weak acids and acidify the cytoplasm of growing pollen tubes (see Supplemental Figure 9 online) but a cytosolic acidification per se, for example through acetate, does not have an effect on anion currents (see Supplemental Figure 8 online) or pollen growth (see Supplemental Figure 9 online). This demonstrates that both channel blockers specifically block S-type anion channels under our experimental conditions. To investigate the in vivo function of SLAH3, CPK2, and CPK20, we isolated T-DNA insertion lines of SLAH3 (see Supplemental Figure 10 and Supplemental Table 5 online), CPK2, and CPK20 alleles (see Supplemental Figure 11 and Supplemental Table 6 online). We performed voltage clamp experiments with *slah3-1* (GABI 371G03), *slah3-2* (SALK_085191) as well as double *cpk2-1 cpk20-2* (SALK_059237 and SALK_073448) mutants and recorded anion currents in pollen tubes grown in chloride as well as nitrate-based medium. We used double *cpk2-1 cpk20-2*

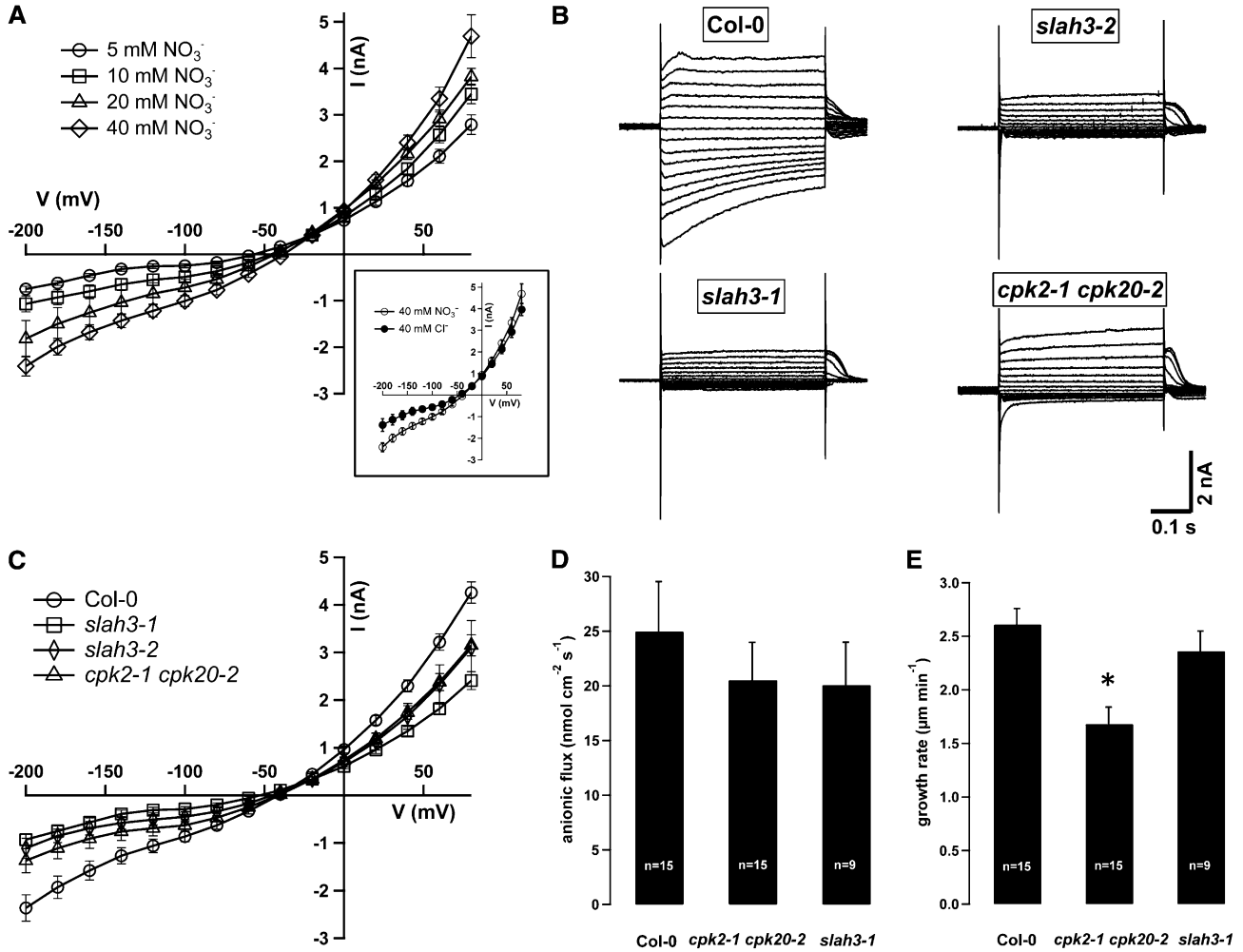

Figure 7. Reduced Anion Currents and Fluxes in *slah3-1, slah3-2*, and *cpk2-1 cpk20-2* Pollen Tubes.

(A) Comparison of steady state pollen tube anion currents in NO_3^--based medium upon application of 400-ms voltage steps from −200 mV to +80 mV (Δ20 mV) when the solution contained 5 mM (○, *n* = 10), 10 mM (□, *n* = 10), 20 mM (△, *n* = 11), or 40 mM NO_3^- (◇, *n* = 10). The inset shows a comparison of the steady state currents in 40 mM Cl^--based medium (●, *n* = 12) or 40 mM NO_3^--based medium (○, *n* = 10).

(B) Current traces of representative *Arabidopsis* wild-type Col-0 (top left), *slah3-1* (bottom left), *slah3-2* (top right), and *cpk2-1 cpk20-2* (bottom right) pollen tubes grown in medium containing 40 mM NO_3^-. Note the strongly and moderately reduced anion currents in *slah3-1, slah3-2*, and *cpk2-1 cpk20-2* double mutant pollen tubes.

(C) Steady state pollen tube anion currents in NO_3^--based medium (40 mM) from wild-type Col-0 (○, *n* = 27), *slah3-1* (□, *n* = 12), *slah3-2* (◇, *n* = 10), and *cpk2-1 cpk20-2* (△, *n* = 13) pollen tubes.

(D) Anion fluxes at the pollen tube tip of wild-type (*n* = 15, Col-0), *cpk2-1 cpk20-2* (*n* = 15), and *slah3-1* (*n* = 9) pollen tubes measured with anion-selective microelectrodes.

(E) Growth rate of the pollen tubes presented in **(D)**. *P ≤ 0.01 (paired Student's *t* test). See the Results for statistical analysis of **(A) and (C)**.

mutants to avoid gene redundancy, because CPK2 and CPK20 are both expressed in pollen tubes and closely related proteins (63% amino acid identity). Similar to patch-clamp analysis of anion currents in lily pollen tube protoplasts (Tavares et al., 2011a), our analysis revealed depolarization-activated, slowly deactivating currents in wild-type Columbia-0 (Col-0), whereas typical S-type anion currents were absent or strongly reduced in *slah3-1, slah3-2*, and *cpk2-1 cpk20-2* mutant cells (Figure 7B). A plot of the steady state currents from membrane voltages clamped from −200 mV to +80 mV (Δ = 20 mV) revealed significantly reduced anion currents in *slah3-1*-, *slah3-2*, and *cpk2-1 cpk20-2* pollen tubes in both chloride-based (see Supplemental Figure 12 online) and nitrate-based solution, pointing to a function for CPK2 and CPK20 in S-type anion channel regulation (Figure 7C). The steady state currents were significantly reduced ($P \leq 0.05$; all statistics by paired Student's *t* test) in *slah3-1* at voltages from −200 to −60 mV and 0 to +80 mV and in *slah3-2* at voltages from −200 to −40 mV and 0 to +80 mV, whereas the currents recorded for *cpk2-1 cpk20-2* were significantly reduced from −200 to −160 mV and from 0 to +80 mV. The steady state current of Col-0 wild-type pollen was

−2.4 ± 0.3 nA (n = 27), that of *cpk2-1 cpk20-2* pollen was −1.4 ± 0.3 nA (n = 12), and those of *slah3-1* and *slah3-2* pollen were −0.9 ± 0.1 nA (n = 13) and −1.1 ± 0.2 nA (n = 10), respectively, at a membrane potential of −200 mV (Figure 7C). Tip-focused anion efflux was quantified by means of ion-selective vibrating microelectrodes in *Arabidopsis* wild-type Col-0, *slah3-1*, and *cpk2-1 cpk20-2* double mutant pollen tubes. In contrast with mean anion fluxes of 24,958 ± 4589 pmol cm^{-2} s^{-1} in wild-type Col-0 (n = 15), *slah3-1* and *cpk2-1 cpk20-2* double mutant pollen tubes were characterized by reduced anion fluxes with 20,059 ± 3936 pmol cm^{-2} s^{-1} (n = 9) and 20,528 ± 3454 pmol cm^{-2} s^{-1} (n = 15), respectively (Figure 7D). However, because of the great variation in fluxes, we could not confirm this variation to be statistically significant. Pollen tubes of *slah3-1* and *cpk2-1 cpk20-2* double mutants demonstrated a reduced growth rate compared with Col-0 (Figure 7E). Mean growth rates of 2.57 ± 0.18 µm s^{-1} in the wild type were recorded, whereas slah3-1 was characterized by a growth rate of 2.36 ± 0.19 µm s^{-1}, and that of *cpk2-1 cpk20-2* mutants was significantly reduced to 1.68 ± 0.16 µm s^{-1} ($P \leq 0.01$).

DISCUSSION

Correlation between Anion and Ca^{2+} Homeostasis

Numerous studies have demonstrated that variations of extracellular ion concentrations of both anionic and cationic nature can profoundly alter pollen tube growth characteristics and germination rate (Weisenseel et al., 1975; Holdaway-Clarke et al., 1997; Fan et al., 2001; Matveyeva et al., 2003). Hence, much attention has been drawn to the role of cations, namely H^+, Ca^{2+}, and K^+, in pollen tube growth. The cytoplasmic H^+ gradient is thought to bear signaling functions for directional growth. It is worth noting that the activities of K^+ channels present in pollen, namely the SPIK, the Two-Pore K^+-channel and the Stelar Outward Rectifying K^+-channel, were reported to be highly dependent on pH, whereas the latter two channels are sensitive to intra-, SPIK is sensitive to extracellular pH changes (Lacombe et al., 2000; Mouline et al., 2002; Becker et al., 2004). Although these K^+ channels could represent target proteins affected by the pH gradient, a correlation between tip-focused pH alterations and K^+ fluxes has not been demonstrated thus far. A plethora of possible functions have been attributed to the well-described tip-focused $[Ca^{2+}]_{cyt}$ gradient in growing pollen tubes. This includes the role of the Ca^{2+} gradient in regulating cytoskeleton integrity and organization (Wang et al., 2008a; Zhang et al., 2010) or membrane trafficking (Camacho and Malhó, 2003). The activity of the K^+-inward rectifier SPIK was recently demonstrated to be CPK dependent (Zhao et al., 2013). Likewise, it is well established that intracellular H^+ and Ca^{2+} gradients generated at the pollen tube tip are closely linked to pollen tube guidance, growth direction, and speed (Pierson et al., 1996; Holdaway-Clarke et al., 1997; Certal et al., 2008; Michard et al., 2008). Many of these physiological processes are interconnected, rendering the analysis of the Ca^{2+} signaling cascades difficult. The current knowledge on generating Ca^{2+} gradients and decoding Ca^{2+} signatures in pollen tubes has recently been comprehensively reviewed (Konrad et al., 2011; Steinhorst and Kudla, 2012). Much less is known about the role of anions on pollen germination and tube growth performance (Tavares et al., 2011b). A negligible role for chloride in the polar growth process was claimed by early studies, using an allegedly anion-free pollen tube growth medium (Weisenseel and Jaffe, 1977). However, after rehydration and during germination, a prominent release of anions into the growth medium can be detected within minutes and provides an anion containing microenvironment (Zonia et al. 2002; Matveyeva et al., 2003). Extracellular flux measurements on the basis of ion-selective electrodes with the vibrating probe technique could identify a close anion flux circuit at the pollen tube apex, which was essential for growth. This anion flux circuit is characterized by a nonoscillatory anion influx 20 to 60 µm behind the tip and a massive oscillatory efflux at the extreme apex (Zonia et al., 2002). The distinct anion fluxes already indicate a functional separation of plasma membrane anion transport in the pollen tube either by differences in subcellular localization and/or regulation of the underlying transport proteins. Flux patterns in *L. longiflorum* and *N. tabacum* are very similar and the magnitude of extracellular anion fluxes, in both species, is orders of magnitude higher compared with apical cation fluxes. This is an unequivocally strong argument for the importance of anion fluxes not only for counterbalancing cation fluxes to maintain electroneutrality but to fulfill other, yet unknown functions. In fact, growth velocity and anion fluxes share approximately the same phase and frequency during oscillatory growth cycles, pointing to a tight coupling of the two parameters, hypothesized as being a reflection of the chloride-driven water transport (Zonia et al., 2002). The molecular nature of S-type (Negi et al., 2008; Vahisalu et al., 2008) and R-type anion channels (Meyer et al., 2010) was discovered only recently, and opens up the possibility of studying the role of anion channels in polar growth. Here we show that the presence of different anion concentrations has profound effects on pollen tube growth performance. Changing the extracellular Cl^- concentration from 0.4 mM to 50 mM Cl^- resulted in 18% wider tube diameters, a reduction in growth velocity, and the emergence of robust growth oscillations.

Furthermore, live-cell imaging experiments employing the *Chloride-Sensor* in this study identified a cytosolic anion gradient strictly following extracellular anion concentration changes (Figure 1). This cytosolic anion gradient matched the plasma membrane anion fluxes, as described by Zonia et al. (2002), and currents, as described by Tavares et al. (2011a). The cytosolic gradient was characterized by high chloride concentration in a cytosolic domain ranging from ~20 to ~40 µm behind the tip. Around that volume, concentrations decreased either drastically toward the growing tip (0 to 15 µm, where the maximal extracellular efflux can be detected) or toward the grain (starting at ~50 to 100 µM behind the tip) (Figure 1). A subsequent rise in cytosolic anion concentrations upon extracellular Cl^- elevation in the region ~20 to 40 µm behind the tip is a hint for an active inward-directed anion translocation process. An anion-H^+ symporter, which was already postulated to exist in root hair cells (Felle, 1994), or cation-chloride co-transporter1 (Colmenero-Flores et al., 2007) represent good candidates for mediating anion influx in that region, but the mechanism remains speculative. Tip-focused anion and Ca^{2+} concentration transients were strictly accompanied by growth oscillations if changes in the extracellular Cl^- concentration exceeded 10 mM (Figures 1 and 2). Interestingly, both the cytosolic anion and Ca^{2+} gradients were eliminated by the application of the anion channel

inhibitor NPPB, which results in the immediate cessation of tube growth. This observation suggests that there is a strong link between anion and Ca^{2+} homeostasis, a notion that is further supported by the fact that the start of oscillatory growth cycles is accompanied by a tip-focused increase of $[Ca^{2+}]_{cyt}$ and a simultaneous reduction in cytosolic anion concentration (Figures 1 and 2). This strengthens the hypothesis that a $[Ca^{2+}]_{cyt}$-dependent anion release at the pollen tube tip generates a cytosolic anion concentration gradient (Figure 8). Indeed, Ca^{2+}-dependent anion currents were recently identified with the patch-clamp technique in both pollen grains and tube protoplasts (Tavares et al., 2011a). The stimulation of anion currents through Ca^{2+} is likely to be an indirect rather than a direct binding of the second messenger to the channels, because of the following: the known anion channels in plants do not exhibit EF hands; various kinase inhibitors suppress anion channel activity in guard cells (a well-established model cell system in terms of anion transport with striking similarity to electric properties of pollen), which also express SLAH3 (Schmidt et al., 1995; Pei et al., 1997); and direct Ca^{2+} binding to anion channels with excised patches (inside-out) in patch-clamp experiments have not been reported. Interestingly, direct Ca^{2+} binding to members of the animal Ca^{2+}-activated anion channel family has been shown. However, these proteins lack typical Ca^{2+} binding motifs such as EF hand domains (Schroeder et al., 2008). In fact, kinase inhibitors have also been shown to influence pollen germination and growth orientation (Moutinho et al., 1998), but effects of kinase inhibitors on pollen tube ion fluxes have not yet been reported.

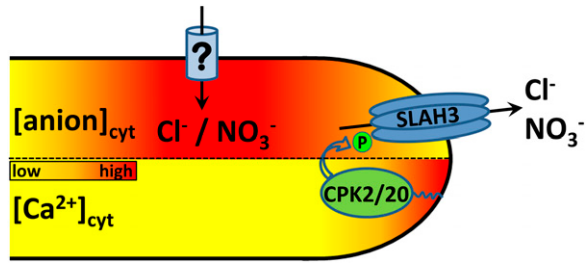

Figure 8. Model of the Link between Cytosolic Anion and Ca^{2+} Concentration at the Tip.

Tip-localized CPK2 and CPK20 are activated by the high $[Ca^{2+}_{free}]_{cyt}$ at the pollen tube apex. A phosphorylation-dependent activation of SLAH3 by these two kinases takes place exclusively at the pollen tube tip. SLAH3-opening generates a cytosolic concentration gradient with low anion concentrations at the tip. An import of anions at the shank, symbolized by relative high cytosolic anion concentrations, is mediated by yet unknown anion transport proteins. Simplistically, the delays on the oscillatory phases of cytosolic Ca^{2+} and Cl^- concentrations could be hypothesized to result from diffusional delays and critical concentration thresholds. This spatial pattern would thus be an emergent property of a double feedback loop of regulation based on the physical properties of these ions.

[See online article for color version of this figure.]

Colocalization and Interaction of SLAH3 with CPK2/20

The molecular identity and function of most channels and transporters mediating ion fluxes in distinct regions of the pollen tube are still unknown. On the basis of qRT-PCR, we were able to determine that the anion channel SLAH3 is expressed in pollen tubes. YFP fusion and transient expression localized SLAH3 uniformly at the plasma membrane (Figure 3D). In line with the finding that SLAH3 activation in stomatal guard cells and mesophyll cells is mediated via CPKs (Geiger et al., 2011), we also identified the pollen-expressed CPK2, CPK20, CPK17, and CPK34 as potential candidates for SLAH3 activation on the basis of microarray data and their subcellular localization. Among the pollen-expressed CPKs investigated, only these kinases exclusively localized at the plasma membrane of the pollen tube tip (Figure 4). We demonstrated the importance of CPK2, CPK20, CPK17, and CPK34 posttranscriptional modifications for their tip localization by mutating the myristoylation and/or palmitoylation sites (see Supplemental Figure 5 online). Biochemical analysis by Lu and Hrabak (2002) concluded that CPK2 was mainly localized at the endoplasmic reticulum. The same authors demonstrated CPK2 myristoylation at the second amino acid, but received only a 50% decrease of the protein content in the membrane fraction upon mutating this residue (G2A), which abolished myristoylation (Lu and Hrabek, 2002). Another biochemical study on CPK localization demonstrated that CPK2 is associated with the membrane fraction only and revealed its high Ca^{2+} sensitivity (Boudsocq et al., 2012).

Transient expression of SLAH3:YFP alone, or coexpression of CPK34 and SLAH3 BiFC constructs, resulted in normal pollen tube growth, whereas coexpression of CPK2 (CPK2:YN) and SLAH3 (YC:SLAH3) BiFC constructs resulted in collapsing pollen tubes in most cases and showed a fluorescence complementation exclusively at the plasma membrane at the tip (see Supplemental Figure 6 online). This result is suggestive of the formation of a functional SLAH3/CPK2 or CPK20 complex at the pollen tube tip. This interaction of the Ca^{2+} activated kinase and channel was confirmed using both fluorescence imaging and electrophysiological methods to identify protein–protein interactions between SLAH3 and CPKs localized at the tip. In transiently transformed pollen tubes, however, the identification of SLAH3 interacting partners using BiFC was not conclusive because of possible false positive BiFC data, even though we did use an advanced BiFC design known to minimize interaction artifacts (Lin et al., 2011) (see Supplemental Figure 6 online). These putative BiFC artifacts in pollen tubes were most likely a consequence of protein overexpression. However, it is worth noting that false- positive fluorescence complementation results in *X. laevis* oocytes occur rather rarely (Geiger et al., 2009a). We thus decided to perform interaction studies combining the more advanced FRET-FLIM and TEVC techniques in *Arabidopsis* mesophyll protoplasts and *X. laevis* oocytes, respectively. Although it is technically challenging, the FRET-FLIM technique represents a superior spectroscopic method for characterizing protein–protein interactions (i.e., FRET with acceptor photobleaching or sensitized emission) because it is thought to be relatively more independent of artifacts (Miyawaki, 2011). We detected a specific interaction and activation of SLAH3 through CPK2 and CPK20 (Figures 5 and 6), whereas CPK17 and CPK34 turned out to behave like negative controls despite their similar subcellular localization. The interaction of CPK2 and CPK20 with SLAH3 was statistically significant ($P \leq 0.0002$) in the FRET-FLIM dataset. However, the positive control (both with CFP:YFP

and mTurquoise/Venus protein pairs) showed a more than 10 times higher average lifetime reduction. This great difference in average fluorescence lifetime reduction is likely a consequence of the transient nature of CPK binding to target proteins in contrast with a constant one in the CFP:YFP fusion protein. The FRET-FLIM data matched the electrophysiological and BiFC data in *Xenopus* oocytes (Figure 6), which is strong evidence for a specific interaction of CPK2 and CPK20 with SLAH3 at the pollen tube tip (Figure 8). FRET-FLIM experiments in planta are still rare and thus there are no comparable FLIM studies, to our knowledge, that used the same fluorophore combination we used (mTurquoise/Venus). We used mTurquoise as the donor for FRET-FLIM because it is an optimized CFP version with a high quantum yield and it harbors a monoexponential decay curve allowing straightforward FLIM analysis (Goedhart et al., 2010).

Anion Current Reduction in *slah3-1*, *slah3-2*, and *cpk2-1 cpk20-2* Pollen Tubes

The TEVC technique was used to perform voltage clamp experiments in pollen tubes with double-barreled electrodes. To resolve anion channel–mediated currents, a potassium-free medium composition was chosen to minimize K^+-channel background activity (see Supplemental Figure 7 online). Using different anion compositions, we were able to resolve channel activity with time-dependent deactivation kinetics, typically for S-type anion channel characteristics of SLAH3 (Geiger et al., 2011). The currents increased in an anion concentration-dependent manner (Figure 7) and could be blocked by two anion channel inhibitors, namely NA and NPPB (see Supplemental Figure 8 online). In line with the selectivity profile of SLAH3, inward currents were increased in NO_3^- compared with Cl^- medium (Figure 7). The higher currents in NO_3^--based medium are most likely the consequence of a higher permeability to NO_3^- versus Cl^- and the shift in channel open probability, a unique feature of SLAH3, as reported by Geiger et al. (2011). A significant reduction of the anion currents in both NO_3^- medium and Cl^- medium was detected in *slah3-1* (~61% and ~46% reduction, respectively), *slah3-2* (~49% in NO_3^- medium), and *cpk2-1 cpk20-2* (~42% and ~38% reductions, respectively) mutant pollen tubes. These results suggest that SLAH3, activated through CPK2 and CPK20, is responsible for anion currents in pollen tubes. A stronger anion current reduction in the *slah3-1, slah3-2*, and cpk2-1 *cpk20-2* mutants was thus detected in NO_3^- medium, because pollen tubes possess a relatively high portion of SLAH3 activity with respect to other anion channel activity. However, we uncovered the existence of at least two other distinct pollen tube anion current characteristics in patch-clamp analysis (Tavares et al., 2011a). Meyer et al. (2010) already demonstrated R-type anion channel ALMT12 expression in pollen via promotor::GUS expression and we confirmed this in our quantitative RT-PCR analysis (Figure 3A). ALMT12 or hitherto unidentified anion channels may thus be possible candidates for the remaining anion currents in *slah3-1* or *slah3-2* pollen tubes.

What Is the Role of Anion Currents during Pollen Tube Growth?

Several transcriptomic analyses showed that more than 450 transporter genes are expressed during pollen germination and pollen tube growth (Pina et al., 2005; Wang et al., 2008b). However, only a few ion transport proteins have been affiliated with gene function to date. The contribution of two predicted cation/H^+ exchangers (CHX), CHX21 and CHX23, with a role in K^+ homeostasis, was demonstrated to be essential for guidance but not for regular pollen tube growth (Lu et al., 2011). An inward rectifying (SPIK) and a weak inward rectifying Two-Pore K^+-channel seem to be responsible for K^+ uptake by pollen grains and tubes (Mouline et al., 2002; Becker et al., 2004; Zhao et al., 2013). A plasma membrane Ca^{2+} pump, ACA9, localized at the plasma membrane is required for normal pollen tube growth and fertilization (Schiøtt et al., 2004). Mutation of a putative Ca^{2+}-permeable channel from the cyclic nucleotide-gated channel family (CNGC18) produces a strong pollen tube phenotype (Frietsch et al., 2007). More recently, the GLR family was implicated in generating the tip-focused $[Ca^{2+}]_{cyt}$ gradient and regulating pollen tube growth in *Arabidopsis* and tobacco (Michard et al., 2011).

Here we shed light on the role of Ca^{2+} signal processing via two CPKs, CPK2 and CPK20, in regulating the anion channel SLAH3 to facilitate pollen tube growth. It is likely that the CPK2/CPK20-driven SLAH3 activation is, at least in part, responsible for generating the steep apical cytosolic anion gradient we identified here. The role and regulation of anion efflux in osmotic pressure-driven movement in guard cells is much better understood (Roelfsema and Hedrich, 2005; Roelfsema et al., 2012) and there, Ca^{2+}-dependent as well as independent signaling pathways exist to activate R- and S-type anion channels (Levchenko et al., 2005; Marten et al., 2007). R- and S-type channel-driven anion efflux leads to plasma membrane depolarization and in turn to the activation of voltage-dependent plasma membrane K^+ channels. A massive release of anions and cations results in the passive efflux of water and consequently in a turgor pressure decrease, which causes stomatal closure. In pollen tubes, the formation of a balloon-like expansion of the pollen tube tip is associated with abolishing tip anion efflux by anion channel inhibitors (Zonia et al., 2002). This observation indicates an anion flux driven balance of the osmotic pressure. A difference in osmotic pressure during oscillatory growth performance or along the cell was controversially discussed recently (Zonia and Munnik, 2007; Winship et al., 2010, 2011). On a strictly biophysical basis, differences in turgor pressure along the cell can theoretically not exist and would require a rather stiff and non-aqueous cytoplasm. In addition, pressure probe measurement attempts failed to detect a correlation between osmotic pressure and growth rates during pollen tube elongation (Benkert et al., 1997).

The effect of anion release, or more generally speaking, of any ion extrusion from the cell via channels will not only lead to changes in osmotic potential but also to changes in the electric potential (if these fluxes are not counter-balanced through simultaneous fluxes of oppositely charged ions in the same direction or of ions with the same charge in opposite directions). A difference in electric polarization of the plasma membrane of growing pollen tubes has recently been reported (Breygina et al., 2009) using spectroscopic techniques and could explain the differential channel activity of voltage-dependent K^+ and Ca^{2+} channels, reported to exist in the pollen tube plasma membrane (Fan et al., 2001; Mouline et al., 2002; Wang et al., 2004; Shang et al., 2005; Qu et al., 2007; Wu et al., 2007). This is a tantalizing hypothesis, because it would permit the generation of the biophysical conditions necessary for

differential plasma membrane polarization domains, a mechanism we are currently trying to address. If proven correct, it would be the first demonstration of such a spatial regulation of steady electric fields at the cellular level, with important consequences on our understanding of cell differentiation and development.

METHODS

Plant Material, Growth Conditions, and Media

Arabidopsis thaliana ecotype Col-0 plants were grown on soil and cultivated in growth chambers for 4 to 6 weeks under short-day conditions (8 h light/16 h darkness, 22/16°C) and after that in a greenhouse in long-day conditions (12 h light/12 h darkness, 22/16°C) with illumination provided by 100 μmol m^{-2} s^{-1} fluorescent tubes (25 W, 230 V, Osram TL70 F32T8/TL 741; Philips). Unless otherwise stated, experiments were performed using *A. thaliana* ecotype Col-0 as wild type. In the case of transcript quantification, the pollen tube growth medium was composed of the following (in mM): 1 MES, 1.6 H_3BO_3, 1 KCl, 3 $CaCl_2$, and 7 $CaNO_3$. The standard medium for electrophysiological measurements with *Arabidopsis* pollen tubes consisted of the following (in mM): 1 MES, 1.6 H_3BO_3, and either 20 $CaCl_2$ or 20 $CaNO_3$. For media with different anion concentrations, $Ca(gluconate)_2$ was used to ensure unaltered Ca^{2+} concentrations. TEVC measurements of *Arabidopsis* pollen were performed in medium containing the following (in mM): 1 MES, 1.6 H_3BO_3, supplemented with either 1 or 10 K-Gluconate to resolve K^+-channel activity. Osmolarity of all *Arabidopsis* pollen media was adjusted to 370 mosmol kg^{-1} (Vapor Pressure Osmometer 5520; Wescor) with D(+)-Suc and pH was adjusted to 6.5 with Tris.

Tobacco (*Nicotiana tabacum* cultivars Petit Havana SR1) plants were grown on soil with a day/night regime of 10 h/14 h, and a temperature of 22 to 24/20 to 22°C provided by a 30 klux white light (SON-T Agro 400W; Philips) until flowering for pollen collection. Pollen used in all assays was collected from anthers immediately after anthesis and used fresh or frozen at −20°C. Tobacco pollen germination medium consisted of the following (in mM): 1 MES, 0.2 $CaCl_2$, and 1.6 H_3BO_3. The pH was adjusted to 5.8 with Tris and osmolarity was adjusted to 400 mosmol kg^{-1} (Vapor Pressure Osmometer 5520) with D(+)-succhrose. Essentially, Ca^{2+} was kept constant and K^+ was not added to the medium for the application of different Cl^- concentrations. To elevate Cl^- only, we adjusted its concentration with HCl and buffered the medium with Tris. Osmolarity was kept the same in all Cl^- solutions and was adjusted with Suc. Suc content in the medium with 50 mM chloride was ~11%. Thus, we assumed that we were working with Suc concentrations that were saturating in terms of Suc-transporter capacity in all media.

For transient transformation of mesophyll protoplasts, *Arabidopsis* ecotype Col-0 plants grown on soil were kept under short-day conditions for 4 to 5 weeks. Mesophyll protoplasts were prepared using the tape-*Arabidopsis* sandwich method (Wu et al., 2009).

In TEVC studies, oocytes were perfused with Tris/MES buffers. The standard solution contained the following (in mM): 10 MES/Tris (pH 5.6), 1 $Ca(gluconate)_2$, 1 $Mg(gluconate)_2$, 100 $NaNO_3$, and 1 $LaCl_3$. Osmolality was adjusted to 220 mosmol/kg with D-sorbitol.

Transient Pollen Transformation

Particle bombardment was performed using a homemade biolistic device similar to the PDS-1000/He biolistic system (Bio-Rad). A 4.3-way valve allowed application, hold, and release of the vacuum (–0.8 bar) to the chamber while a magnetic valve controlled helium-pressure (8–9 kp/cm^2) pulse injection. Approximately 2.5 mg tungsten particles (Bio-Rad) of 1.0-μm diameter were coated with 10 μg plasmid DNA according to the Bio-Rad instruction manual (Sanford et al., 1993). Particles diluted in water were placed on a filter (VWR International GmbH) screwed in position right behind the pressure valve. The parameters of particle travel distance were as follows: 7 cm between the filter and a grid (0.5-mm mesh width) and 5 cm between the grid and the pollen. Bombardment of hydrated *N. tabacum* pollen grains (either fresh or frozen) was spotted on 1% agarose plates containing standard tobacco growth medium. After transformation, tobacco pollen were transferred to dishes glued to precision cover slips of 0.17 ± 0.1 mm (Assistent) previously coated with 0.01% poly(L-Lys) (Sigma-Aldrich) and mixed with 40°C warm tobacco medium containing low melt agarose (Carl Roth) resulting in a final agarose concentration of 1%. On a 40°C hot plate, pollen grains were allowed to sink to the bottom of cover slip glass, needless medium was discarded, and the remaining medium was allowed to solidify at room temperature. This procedure allowed pollen tubes to grow on the surface of the cover slip, in a manner that was suitable for imaging.

Live-Cell and Confocal Imaging

Widefield-imaging of *N. tabacum* pollen tubes was performed on an inverted Zeiss microscope AxioObserver (Carl Zeiss AG). Hardware and data management were performed via VisiView software (Visitron Systems). Fluorophores were excited with the VisiChrome High-Speed Polychromator System (Visitron Systems). Fluorescence was captured through either a ×40 or ×60 objective (C-Apochromat 40×/1.2 W Korr or C-Apochromat 63×/1.20 W Korr; Carl Zeiss) and a 512 × 512 pixel Evolve EMCCD camera (Photometrics). For CFP or YFP illumination, excitation wavelengths of 420 nm or 505 nm were used, respectively, and fluorescence emission was reflected via a dual-band dichroic mirror 440/520 and filtered with a dual-band emitter 464/547 (Semrock Inc.). A 6-position high-speed filter wheel (Ludl Electronic Products Ltd.), mounted at the side port, equipped with a CFP (ET 470/24 nm) and YFP (ET 535/30 nm) bandpass filter (Chroma Technology Corporation,), was used to separate the emission wavelengths of CFP and YFP. For YC3.6 illumination, CFP emission was recorded under CFP excitation at 420 nm (CFP@CFP) and YFP under CPF excitation (YFP@CFP). The Cl^- sensor was illuminated the same way and YFP was recorded at YFP excitation (YFP@YFP) and ratio analysis was performed with three channels. Because the emission spectrum of eYFP, the fluorescence FRET acceptor protein in the Cl^- sensor, is dependent on H^+ concentrations (McAnaney et al., 2005), the YFP@CFP/CFP@CFP ratio of the Cl^- sensor possesses degrees of pH dependency originating from the pH gradient in pollen tubes. To subtract the pH dependency of the FRET ratio signal, the YFP@CFP channel was divided by the YFP@YFP channel prior to the division by the CFP@CFP channel, which is pH independent (Sawano and Miyawaki, 2000). The pH-probe *pHluorin* was excited at 390 nm and 470 nm and emission was filtered through a dichroic mirror (500 nm) and bandpass filter (HQ 535/25 M; AF Analysentechnik). Image processing was performed using MacBiophotonics ImageJ v1.46 (National Institute of Health). Simultaneous pollen tube growth and ratio analysis were performed with a self-made script for the Octave 3.2.4 free software (http://www.gnu.org/software/octave/). Data were processed and plotted with Igor Pro 5.02 software (Wavemetrics Inc.). Because of the probe photobleaching and phototoxicity that occur during long-term live-cell imaging experiments, we were not able to determine cross-correlation in the subsecond range between the cytosolic anion as well as Ca^{2+} and H^+ gradients and growth velocity in detail.

For documentation of the oocyte BiFC results and the subcellular localization of CPK2:YFP in *Arabidopsis* pollen tubes, images were taken with a confocal laser scanning microscope (TCS SP5 II; Leica Microsystems) equipped with Leica HCX IRAPO 25×/0.95 and HCX PL APO 63×/1.20 W CORR CS objectives, respectively.

Electrophysiology

Voltage clamp experiments on pollen tubes were performed by impalement with double-barreled electrodes using a drift-free piezo-driven Sensapex Micromanipulator. Double-barreled electrodes were pulled from two

borosilicate capillaries with filament (outer diameter 1 mm, inner diameter 0.58 mm; Hilgenberg). The two capillaries were aligned, heated, and twisted 360° in a customized vertical electrode puller (L/M-3P-A; List Medical Electronic) and finally pulled on a horizontal laser puller (P2000; Sutter Instruments), as described previously (Becker et al., 2004). Both barrels were filled with 300 mM KCl and connected by means of Ag/AgCl wires to the microelectrode amplifier (TEC-05X; NPI Electronic) equipped with head stages of $\geq 10^{13}\ \Omega$ input impedance. Voltage clamp protocols were applied with PULSE software (HEKA Electronics). Data were low pass-filtered at 2 kHz and sampled at 1 kHz. *Arabidopsis* pollen tubes were grown on the top of a semisolid medium containing 1.5% low-melt agarose. To ensure a high germination rate, only freshly opened flowers were used and dipped on the surface of the semisolid medium. Germinated pollen tubes were covered with liquid medium 2 to 3 h after dipping in medium with the same composition (for media composition see the section on plant material, growth conditions, and media), prior to electrode impalement. After impalement, the membrane potential was recorded until values reached a plateau, usually within 10 to 30 s. Pollen tubes were voltage clamped at the free running membrane potential only to perform current recordings and when voltage pulses in the range of −200 mV to +80 mV (Δ20 mV increments) were applied.

TEVC recordings were performed with *Xenopus laevis* oocytes 2 to 3 d after cRNA injection with a Turbo TEC-01C amplifier (NPI Electronic). The electrodes were filled with 3 M KCl and had typical input resistances of 2 to 6 MΩ. Voltage clamp protocols were applied with Patchmaster software (HEKA Electronics). Starting from a holding potential of 0 mV, single 20-s voltage pulses were applied in 20-mV decrements from +60 to −200 mV followed by a 3-s voltage pulse to −120 mV. Instantaneous currents (I_{inst}) were extracted directly after the voltage jump from the holding potential of 0 mV to 50-ms test pulses ranging from +70 to −150 mV. Data points with error bars represent the mean ± SD, and statistical significance was verified by a paired Student's *t* test.

Extracellular anion flux measurements were performed as follows. *Arabidopsis* pollen grains were collected from fresh flowers and germinated in liquid medium containing the following: 500 μM KCl, 500 μM $CaCl_2$, 125 μM $MgSO_4$, 500 μM H_3BO_3, 125 μM HEPES, and 15% of Suc at pH 7.5. After at least 3 h of incubation at 21.5°C, measurements were performed on growing pollen tubes that were at least 150 μm in length. The respective growth rate was evaluated simultaneously with the extracellular anionic fluxes, defined as the total length grown during the experiment divided by the amount of time spanned. Extracellular anionic flux at the pollen tube tip was estimated with the ion-selective vibrating probe (Kühtreiber and Jaffe, 1990; Shipley and Feijó, 1999). Anion-specific microelectrodes were fabricated from 1.5-mm borosilicate glass capillaries and pulled with a Sutter P-97 electrode puller (Sutter Instruments), baked at 230°C overnight and then internally covered with *N*,*N*-dimethyltrimethylethylsilamine (Sigma-Aldrich) for 40 min. Electrodes were backfilled with 100 mM KCl and subsequently front-loaded with a 30-μm column of the anion-selective liquid cocktail (chloride ionophore I cocktail A; Sigma-Aldrich). A silver/silver chloride wire was inserted into the back of the electrode and a dry electrode (DryRef-2; World Precision Instruments) was used as a reference. Electrode calibration was performed by measuring the Nernst potential of three different Cl^- concentration solutions (0.1, 1, and 10 mM KCl). Electrode positioning and vibrating was performed with a stepper-motor–driven three-dimensional positioner. Data acquisition, setting of the voltage parameters, and the three-dimensional electrode micromanipulator were controlled via ASET software (Science Wares and Applicable Electronics). The ion-selective probe vibrated with an excursion of 5 μm, completing the cycle of acquisition in 4 s, which includes a tunable settling time after each move, two measurement periods, and the respective excursion time. All measurements were obtained as close as possible to the tip membrane without touching the tube. Background voltage values were taken after each measurement ~500 μm away from any other pollen grain or tube, and the values were subtracted from the millivolt differential recordings during data processing using a custom made Microsoft Excel sheet. Fluxes were calculated using Fick's law and the chloride diffusion coefficient in aqueous solution at 25°C ($-2.03 \times 10^{-5}\ cm^{-2}\ s^{-1}$).

GUS Staining

A GUS staining assay (Jefferson et al., 1987) was performed on fully opened flowers of the ProSLAH3::GUS reporter gene line grown as described in the section on plant material, growth conditions, and media. Flowers were submerged in 1 mL staining solution (containing the following [in mM]: 100 sodium phosphate buffer pH 7.0, 1 EDTA pH 8.0, 5 potassium ferricyanide, 5 potassium ferrocyanide, 1% Triton-X-100, and 1 mg/ml X-Gluc) and vacuum infiltrated for 5 min. The samples were incubated overnight at 37°C followed by several washing steps with 70% ethanol to destain specimens. Documentation was performed with a Keyence VHX-100k digital microscope and was processed via MacBiophotonics ImageJ v1.46 software.

Quantitative RT-PCR

A. thaliana ecotype Col-0 pollen were collected via the vacuum cleaner method (Johnson-Brousseau and McCormick, 2004) and germinated/grown by placing pollen grain covered-gaze directly on semisolid medium containing 1.5% agarose. After 5 h, the tissue was frozen in liquid nitrogen and ground using glass beads. RNA isolation of pollen tubes was performed using oligo dT Dynabeads (Life Technologies) according to the manufacturer's instructions with some minor modifications. Ground pollen tube samples were mixed with lysis buffer, agitated for 2 min, and centrifuged and the supernatant was then mixed with 30 μL activated Dynabeads. After 30 min on a rotation mixer, beads were washed consecutively with buffer containing lithium dodecylsulfate and with non-lithium dodecylsulfate–containing buffer. After every washing step, the beads were separated from the supernatant by magnetic force. Washed mRNA was eluted from the Dynabeads in 8 μL elution buffer at 72°C. The purified mRNA was subsequently used for cDNA synthesis performed by adding 0.4 μL poly(T) primer (100 μM), 0.5 μL deoxynucleotide triphosphate (10 mM), and 2.5 μL 10× Master Mix, incubated at 72°C for 2 min and then placed on ice. Reverse transcriptase was added and the sample was incubated for 1 h at 42°C. Quantitative RT-PCR was performed according to the Abgene SYBR Green assay in an Eppendorf Realplex cycler. For transcription quantification, cDNA was diluted 1:20 in H_2O containing 10 μg/ml t-RNA. Samples (2 μl) were mixed with 10 μL SYBR Green Mix and a gene-specific primer mix (8 μl). A detailed list of the qRT-PCR primers used is presented in Supplemental Table 3 online. In addition to the pollen cDNA samples, an internal standard curve (range, 1 fg/μl to 0.001 fg/μl) for each gene was quantified. Transcripts were normalized to 10,000 molecules of actin2/8 using standard curves calculated for the individual PCR products.

FRET-FLIM Measurements

FRET-FLIM measurements between mTurquoise (CFP) (Goedhart et al., 2010) and Venus (YFP) (Nagai et al., 2002) were performed as described previously (Russinova et al., 2004) using the Bio-Rad Radiance 2100 MP system combined with a Nikon TE 300 inverted microscope. Two-photon excitation pulses were generated by a Ti:Sapphire laser (Coherent Mira) pumped by a 5-W Coherent Verdi laser. Pulse trains of 76 MHz (150 fs pulse duration, 860 nm center wavelength) were produced. The excitation light was directly coupled to the microscope and focused into the sample using a CFI Plan Apochromat ×60 water immersion objective lens with a numerical aperture of 1.2. CFP emission was detected using the nondescanned single photon counting Hamamatsu HPM-100-40 Hybrid detector (Becker & Hickel), using a 480DF30 bandpass filter. Images with a frame size of 64 × 64 pixels were acquired. Donor fluorescence lifetimes (CFP) were analyzed using SPCImage 3.50 software (Becker and Hickl) and a two-component decay model. The statistical significance of differences

between donor-only and donor-acceptor combinations was determined using Student's *t* test.

Molecular Biology and Cloning

To analyze the subcellular localization of the ion channels and CPKs used in this study, their cDNA was cloned into a plant expression vector as described by Nour-Eldin et al. (2006) with a cloning technique based on a uracil-specific-excision reagent (USER-Friendly) combined with a proof-reading DNA polymerase (Nour-Eldin et al., 2006). The plant expression vector used was based on a pSAT vector containing either the full-length YFP or N- or C-terminal halves upstream or downstream of a USER cassette. Similar to studies described previously (Grefen et al., 2010), gene expression was ensured through the promoter and terminator sequence of the ubiquitin10 and ribulose-1,5-bis-phosphate carboxylase/oxygenase enzyme downstream and upstream of the USER cassette, respectively. The primers used to amplify the cDNAs are listed in Supplemental Table 4 online. Plasmid DNA was amplified in competent *Escherichia coli* mrf′ cells, verified via enzyme restriction as well as sequencing and purification with the Qiagen Midi Kit.

For *X.laevis* oocyte experiments, the cDNAs of SLAH3 as well as EF hand-truncated versions of CPK21, CPK2, CPK20, CPK17, and CPK34 were cloned into oocyte (BiFC) expression vectors (based on pGEM vectors), by an advanced uracil-excision–based cloning technique as described by Nour-Eldin et al. (2006). For functional analysis, cRNA was prepared with the mMESSAGE mMACHINE T7 Transcription Kit (Ambion). Oocyte preparation and cRNA injection were performed as described (Becker et al., 1996). For oocyte BiFC and electrophysiological experiments, 10 ng cRNA was injected each.

The identities of cpk2-1 cpk20-2, slah3-1, and slah3-2 loss-of-function T-DNA insertion *Arabidopsis* lines were verified via PCRs. A detailed description and primer list used for genotyping are presented in Supplemental Tables 5 and 6 online.

Accession Numbers

Sequence data from this article can be found in the *Arabidopsis* Genome Initiative or GenBank/EMBL databases under the following accession numbers: SLAH3:AT5G24030 (Q9FLV9), SLAC1:At1g12480 (Q9LD83), SLAH1:At1g62280 (Q5E930), SLAH2:At4g27970 (Q9ASQ7), SLAH3:At1g62262 (A8MRV9), ALMT12:At4g17970 (O49696), CPK2:At3g10660 (Q38870), CPK6:At2g17290 (Q38872), CPK11:At1g35670 (Q39016), CPK14:At2g41860 (P93759), CPK16:At2g17890 (Q7XJR9), CPK17:At5g12180 (Q9FMP5), CPK20:At2g38910 (Q9ZV15), CPK24:At2g31500 (Q9SIQ7), CPK26:At4g38230 (Q9SZM3), CPK32:At3g57530 (Q6NLQ6), and CPK34:At5g19360 (Q3E9C0).

Supplemental Data

The following materials are available in the online version of this article.

Supplemental Figure 1. Imaging of the $[pH]_{cyt}$ Gradient in Pollen Tubes upon an Increase in Extracellular Chloride Concentration.

Supplemental Figure 2. Subcellular Localization of the SLAH3 Anion Channel.

Supplemental Figure 3. CPK2 and CPK20 Are Expressed in Pollen.

Supplemental Figure 4. Subcellular Localization of CPK2 in *A. thaliana* Pollen Tubes.

Supplemental Figure 5. Subcellular Localization of CPKs Depends on Myristoylation and/or Palmitoylation.

Supplemental Figure 6. Bimolecular Fluorescence Complementation in Pollen Tubes.

Supplemental Figure 7. K^+ Currents of *A. thaliana* Pollen Tubes.

Supplemental Figure 8. Anion Channel Blockers Inhibit Pollen Tube Anion Currents.

Supplemental Figure 9. Imaging of the $[pH]_{cyt}$ Gradient in Pollen Tubes upon Anion Channel Inhibitor Treatment.

Supplemental Figure 10. Identification of a Homozygous SLAH3-1 *Arabidopsis* Line.

Supplemental Figure 11. Identification of a Homozygous cpk2-1 cpk20-2 *Arabidopsis* Line.

Supplemental Figure 12. Reduced Chloride Current in slah3-1 and cpk2-1 cpk20-2 Pollen Tubes.

Supplemental Table 1. Primers Used for Cloning and Generating Stable *Arabidopsis* ProCPK2::GUS and ProCPK20::GUS Lines.

Supplemental Table 2. Calculation of Pollen Tube $[NO_3^-]_{cyt}$ in Different NO_3^- Media Concentrations via the Reversal Potential.

Supplemental Table 3. Primers Used for Quantitative RT-PCR Analysis.

Supplemental Table 4. Primers Used for Cloning and Subcloning.

Supplemental Table 5. Primers Used for Genotyping of the slah3-1 *Arabidopsis* Line.

Supplemental Table 6. Primers Used for Genotyping of the cpk2-1 cpk20-2 *Arabidopsis* Line.

Supplemental Movie 1. Time-Lapse Movie of a Growing *N. tabacum* Pollen Tube, Transiently Expressing the *Cl–Sensor*.

Supplemental Movie 2. Time-Lapse Movie of a Growing *N. tabacum* Pollen Tube, Transiently Expressing Ca^{2+} Indicator YC3.6.

ACKNOWLEDGMENTS

We thank Piotr Bregestowski for sharing plasmid encoding of the Cl^- Sensor, T.W.J. Gadella Jr. for sharing plasmid encoding of mTurquoise, and Karin Schumacher for sharing YC3.6 containing plasmid. The gift of pSLAH3:GUS seeds by Koh Iba is greatly acknowledged and we thank Hussam Nour-Eldin and Anna Barbara Halkier for sharing USER vectors. The development of an Octave script by Dominik Richter to analyze growth velocity and signal intensity is greatly acknowledged. This research was supported by the Foundation for Science and Technology (grants SFRH/BPD/42596/2007 to K.R.K. and PTDC/BEX-BCM/0376/2012 and PTDC/BIA-PLA/4018/2012 to J.A.F.) and Deutsche Forschungsgemeinshaft (Research Unit FOR964 funding to T.R. and grants HE 1640/27-1 and HE 1640/27-2 to R.H.). J.A.F. also acknowledges support from the European COST Action FA0903 on Harnessing Plant Reproduction for Crop Improvement.

AUTHOR CONTRIBUTIONS

K.R.K., R.H., T.R. and J.A.F. designed research; K.R.K., T.G., M.-T.P., R.L., J.-W.B., and T.M. performed research; K.R.K., T.G., M.-T.P., R.L., J.-W.B., and T.M. analyzed data; K.R.K., R.H., and J.A.F. wrote the article and T.R. contributed.

Received September 16, 2013; revised October 17, 2013; accepted October 31, 2013; published November 26, 2013.

REFERENCES

Allen, G.J., Chu, S.P., Harrington, C.L., Schumacher, K., Hoffmann, T., Tang, Y.Y., Grill, E., and Schroeder, J.I. (2001). A defined range of guard cell calcium oscillation parameters encodes stomatal movements. Nature **411:** 1053–1057.

Allen, G.J., Chu, S.P., Schumacher, K., Shimazaki, C.T., Vafeados, D., Kemper, A., Hawke, S.D., Tallman, G., Tsien, R.Y., Harper, J.F., Chory, J., and Schroeder, J.I. (2000). Alteration of stimulus-specific guard cell calcium oscillations and stomatal closing in *Arabidopsis* det3 mutant. Science **289:** 2338–2342.

Becker, D., Dreyer, I., Hoth, S., Reid, J.D., Busch, H., Lehnen, M., Palme, K., and Hedrich, R. (1996). Changes in voltage activation, Cs+ sensitivity, and ion permeability in H5 mutants of the plant K+ channel KAT1. Proc. Natl. Acad. Sci. USA **93:** 8123–8128.

Becker, D., et al. (2004). AtTPK4, an *Arabidopsis* tandem-pore K^+ channel, poised to control the pollen membrane voltage in a pH- and Ca^{2+}-dependent manner. Proc. Natl. Acad. Sci. USA **101:** 15621–15626.

Benkert, R., Obermeyer, G., and Bentrup, F.-W. (1997). The turgor pressure of growing lily pollen tubes. Protoplasma **198:** 1–8.

Boavida, L.C., Vieira, A.M., Becker, J.D., and Feijó, J.A. (2005). Gametophyte interaction and sexual reproduction: How plants make a zygote. Int. J. Dev. Biol. **49:** 615–632.

Boudsocq, M., Droillard, M.-J., Regad, L., and Laurière, C. (2012). Characterization of *Arabidopsis* calcium-dependent protein kinases: Activated or not by calcium? Biochem. J. **447:** 291–299.

Brandt, B., Brodsky, D.E., Xue, S., Negi, J., Iba, K., Kangasjärvi, J., Ghassemian, M., Stephan, A.B., Hu, H., and Schroeder, J.I. (2012). Reconstitution of abscisic acid activation of SLAC1 anion channel by CPK6 and OST1 kinases and branched ABI1 PP2C phosphatase action. Proc. Natl. Acad. Sci. U. S. A. **109:** 10593–10598.

Breygina, M., Smirnova, A., Maslennikov, M., Matveeva, N., and Yermakov, I. (2010). Effects of anion channel blockers NPPB and DIDS on tobacco pollen tube growth and its mitochondria state. Cell Tissue Biol. **4:** 289–296.

Breygina, M.A., Smirnova, A.V., Matveeva, N.P., and Yermakov, I.P. (2009). Membrane potential changes during pollen germination and tube growth. Cell Tissue Biol. **3:** 573–582.

Camacho, L., and Malhó, R. (2003). Endo/exocytosis in the pollen tube apex is differentially regulated by Ca^{2+} and GTPases. J. Exp. Bot. **54:** 83–92.

Camacho, L., Parton, R., Trewavas, A.J., and Malhó, R. (2000). Imaging cytosolic free-calcium distribution and oscillations in pollen tubes with confocal microscopy: A comparison of different dyes and loading methods. Protoplasma **212:** 162–173.

Certal, A.C., Almeida, R.B., Carvalho, L.M., Wong, E., Moreno, N., Michard, E., Carneiro, J., Rodriguéz-Léon, J., Wu, H.M., Cheung, A.Y., and Feijó, J.A. (2008). Exclusion of a proton ATPase from the apical membrane is associated with cell polarity and tip growth in *Nicotiana tabacum* pollen tubes. Plant Cell **20:** 614–634.

Cheng, S.H., Willmann, M.R., Chen, H.C., and Sheen, J. (2002). Calcium signaling through protein kinases. The Arabidopsis calcium-dependent protein kinase gene family. Plant Physiol. **129:** 469–485.

Colmenero-Flores, J.M., Martínez, G., Gamba, G., Vázquez, N., Iglesias, D.J., Brumós, J., and Talón, M. (2007). Identification and functional characterization of cation-chloride cotransporters in plants. Plant J. **50:** 278–292.

Fan, L.-M., Wang, Y.-F., Wang, H., and Wu, W.-H. (2001). In vitro *Arabidopsis* pollen germination and characterization of the inward potassium currents in *Arabidopsis* pollen grain protoplasts. J. Exp. Bot. **52:** 1603–1614.

Feijó, J.A. (1999). The pollen tube oscillator: Towards the molecular mechanism of tip growth? In Fertilization in Higher Plants: Molecular and Cytological Aspects, M. Cresti, G. Cai, and S. Moscatelli, eds (Berlin Heidelberg: Springer-Verlag), pp 317–336.

Feijó, J.A. (2010). The mathematics of sexual attraction. J. Biol. **9:** 18.

Feijó, J.A., Costa, S.S., Prado, A.M., Becker, J.D., and Certal, A.C. (2004). Signalling by tips. Curr. Opin. Plant Biol. **7:** 589–598.

Feijó, J.A., Sainhas, J., Hackett, G.R., Kunkel, J.G., and Hepler, P.K. (1999). Growing pollen tubes possess a constitutive alkaline band in the clear zone and a growth-dependent acidic tip. J. Cell Biol. **144:** 483–496.

Feijó, J.A., Sainhas, J., Holdaway-Clarke, T., Cordeiro, M.S., Kunkel, J.G., and Hepler, P.K. (2001). Cellular oscillations and the regulation of growth: The pollen tube paradigm. Bioessays **23:** 86–94.

Felle, H.H. (1994). The H^+/Cl^- symporter in root hair cells of *Sinapis alba* (an electrophysiological study using ion-selective microelectrodes). Plant Physiol. **106:** 1131–1136.

Frietsch, S., Wang, Y.F., Sladek, C., Poulsen, L.R., Romanowsky, S.M., Schroeder, J.I., and Harper, J.F. (2007). A cyclic nucleotide-gated channel is essential for polarized tip growth of pollen. Proc. Natl. Acad. Sci. USA **104:** 14531–14536.

Geiger, D., Becker, D., Vosloh, D., Gambale, F., Palme, K., Rehers, M., Anschuetz, U., Dreyer, I., Kudla, J., and Hedrich, R. (2009a). Heteromeric AtKC1{middle dot}AKT1 channels in *Arabidopsis* roots facilitate growth under K+-limiting conditions. J. Biol. Chem. **284:** 21288–21295.

Geiger, D., Maierhofer, T., Al-Rasheid, K.A., Scherzer, S., Mumm, P., Liese, A., Ache, P., Wellmann, C., Marten, I., Grill, E., Romeis, T., and Hedrich, R. (2011). Stomatal closure by fast abscisic acid signaling is mediated by the guard cell anion channel SLAH3 and the receptor RCAR1. Sci. Signal. **4:** ra32.

Geiger, D., Scherzer, S., Mumm, P., Stange, A., Marten, I., Bauer, H., Ache, P., Matschi, S., Liese, A., Al-Rasheid, K.A.S., Romeis, T., and Hedrich, R. (2009b). Activity of guard cell anion channel SLAC1 is controlled by drought-stress signaling kinase-phosphatase pair. Proc. Natl. Acad. Sci. USA **106:** 21425–21430.

Geiger, D., Scherzer, S., Mumm, P., Marten, I., Ache, P., Matschi, S., Liese, A., Wellmann, C., Al-Rasheid, K.A., Grill, E., Romeis, T., and Hedrich, R. (2010). Guard cell anion channel SLAC1 is regulated by CDPK protein kinases with distinct Ca^{2+} affinities. Proc. Natl. Acad. Sci. USA **107:** 8023–8028.

Gilroy, S., and Jones, D.L. (2000). Through form to function: Root hair development and nutrient uptake. Trends Plant Sci. **5:** 56–60.

Goedhart, J., van Weeren, L., Hink, M.A., Vischer, N.O.E., Jalink, K., and Gadella, T.W.J., Jr.,. (2010). Bright cyan fluorescent protein variants identified by fluorescence lifetime screening. Nat. Methods **7:** 137–139.

Grefen, C., Donald, N., Hashimoto, K., Kudla, J., Schumacher, K., and Blatt, M.R. (2010). A ubiquitin-10 promoter-based vector set for fluorescent protein tagging facilitates temporal stability and native protein distribution in transient and stable expression studies. Plant J. **64:** 355–365.

Hepler, P.K., and Winship, L.J. (2010). Calcium at the cell wall-cytoplast interface. J. Integr. Plant Biol. **52:** 147–160.

Heslop-Harrison, J.S., Heslop-Harrison, J., Heslop-Harrison, Y., and Reger, B.J. (1985). The distribution of calcium in the grass pollen tube. Proc. R. Soc. Lond. B Biol. Sci. **225:** 315–327.

Holdaway-Clarke, T.L., Feijo, J.A., Hackett, G.R., Kunkel, J.G., and Hepler, P.K. (1997). Pollen tube growth and the intracellular cytosolic calcium gradient oscillate in phase while extracellular calcium influx is delayed. Plant Cell **9:** 1999–2010.

Hrabak, E.M., et al. (2003). The Arabidopsis CDPK-SnRK superfamily of protein kinases. Plant Physiol. **132:** 666–680.

Jefferson, R.A., Kavanagh, T.A., and Bevan, M.W. (1987). GUS fusions: Beta-glucuronidase as a sensitive and versatile gene fusion marker in higher plants. EMBO J. **6:** 3901–3907.

Johnson-Brousseau, S.A., and McCormick, S. (2004). A compendium of methods useful for characterizing *Arabidopsis* pollen mutants and gametophytically-expressed genes. Plant J. **39:** 761–775.

Keller, U.B., Hedrich, R., and Raschke, K. (1989). Voltage dependent anion channels in the plasma membrane of guard cells. Nature **341:** 450–452.

Konrad, K.R., and Hedrich, R. (2008). The use of voltage-sensitive dyes to monitor signal-induced changes in membrane potential-ABA triggered membrane depolarization in guard cells. Plant J. **55:** 161–173.

Konrad, K.R., Wudick, M.M., and Feijó, J.A. (2011). Calcium regulation of tip growth: New genes for old mechanisms. Curr. Opin. Plant Biol. **14:** 721–730.

Kühtreiber, W.M., and Jaffe, L.F. (1990). Detection of extracellular calcium gradients with a calcium-specific vibrating electrode. J. Cell Biol. **110:** 1565–1573.

Lacombe, B., Pilot, G., Gaymard, F., Sentenac, H., and Thibaud, J.B. (2000). pH control of the plant outwardly-rectifying potassium channel SKOR. FEBS Lett. **466:** 351–354.

Lazzaro, M.D., Cardenas, L., Bhatt, A.P., Justus, C.D., Phillips, M.S., Holdaway-Clarke, T.L., and Hepler, P.K. (2005). Calcium gradients in conifer pollen tubes; dynamic properties differ from those seen in angiosperms. J. Exp. Bot. **56:** 2619–2628.

Levchenko, V., Konrad, K.R., Dietrich, P., Roelfsema, M.R., and Hedrich, R. (2005). Cytosolic abscisic acid activates guard cell anion channels without preceding Ca^{2+} signals. Proc. Natl. Acad. Sci. USA **102:** 4203–4208.

Lin, J., Wang, N., Li, Y., Liu, Z., Tian, S., Zhao, L., Zheng, Y., Liu, S., Li, S., Jin, C., and Xia, B. (2011). LEC-BiFC: A new method for rapid assay of protein interaction. Biotech. Histochem. **86:** 272–279.

Lorenzen, I., Aberle, T., and Plieth, C. (2004). Salt stress-induced chloride flux: A study using transgenic *Arabidopsis* expressing a fluorescent anion probe. Plant J. **38:** 539–544.

Lu, Y., Chanroj, S., Zulkifli, L., Johnson, M.A., Uozumi, N., Cheung, A., and Sze, H. (2011). Pollen tubes lacking a pair of K^+ transporters fail to target ovules in *Arabidopsis.* Plant Cell **23:** 81–93.

Markova, O., Mukhtarov, M., Real, E., Jacob, Y., and Bregestovski, P. (2008). Genetically encoded chloride indicator with improved sensitivity. J. Neurosci. Methods **170:** 67–76.

Marten, H., Konrad, K.R., Dietrich, P., Roelfsema, M.R., and Hedrich, R. (2007). Ca^{2+}-dependent and -independent abscisic acid activation of plasma membrane anion channels in guard cells of *Nicotiana tabacum.* Plant Physiol. **143:** 28–37.

Matveyeva, N.P., Andreyuk, D.S., and Yermakov, I.P. (2003). Transport of Cl- across the plasma membrane during pollen grain germination in tobacco. Biochemistry Mosc. **68:** 1247–1251.

McAnaney, T.B., Zeng, W., Doe, C.F.E., Bhanji, N., Wakelin, S., Pearson, D.S., Abbyad, P., Shi, X., Boxer, S.G., and Bagshaw, C.R. (2005). Protonation, photobleaching, and photoactivation of yellow fluorescent protein (YFP 10C): A unifying mechanism. Biochemistry **44:** 5510–5524.

Meyer, S., Mumm, P., Imes, D., Endler, A., Weder, B., Al-Rasheid, K.A., Geiger, D., Marten, I., Martinoia, E., and Hedrich, R. (2010). AtALMT12 represents an R-type anion channel required for stomatal movement in *Arabidopsis* guard cells. Plant J. **63:** 1054–1062.

Michard, E., Alves, F., and Feijó, J.A. (2009). The role of ion fluxes in polarized cell growth and morphogenesis: The pollen tube as an experimental paradigm. Int. J. Dev. Biol. **53:** 1609–1622.

Michard, E., Dias, P., and Feijó, J.A. (2008). Tobacco pollen tubes as cellular models for ion dynamics: Improved spatial and temporal resolution of extracellular flux and free cytosolic concentration of calcium and protons using pHluorin and YC3.1 CaMeleon. Sex. Plant Reprod. **21:** 169–181.

Michard, E., Lima, P.T., Borges, F., Silva, A.C., Portes, M.T., Carvalho, J.E., Gilliham, M., Liu, L.H., Obermeyer, G., and Feijó, J.A. (2011). Glutamate receptor-like genes form Ca^{2+} channels in pollen tubes and are regulated by pistil D-serine. Science **332:** 434–437.

Miesenböck, G., De Angelis, D.A., and Rothman, J.E. (1998). Visualizing secretion and synaptic transmission with pH-sensitive green fluorescent proteins. Nature **394:** 192–195.

Miyawaki, A. (2011). Development of probes for cellular functions using fluorescent proteins and fluorescence resonance energy transfer. Annu. Rev. Biochem. **80:** 357–373.

Moreno, N., Colaço, R., and Feijó, J.A. (2007). The pollen tube oscillator: Integrating biophysics and biochemistry into cellular growth and morphogenesis. In Rhythms in Plants: Phenomenology and Adaptive Significance, S. Mancuso and S. Shabala, eds (Berlin Heidelberg: Springer-Verlag), pp 769–787.

Mouline, K., Véry, A.A., Gaymard, F., Boucherez, J., Pilot, G., Devic, M., Bouchez, D., Thibaud, J.B., and Sentenac, H. (2002). Pollen tube development and competitive ability are impaired by disruption of a Shaker $K(^+)$ channel in *Arabidopsis.* Genes Dev. **16:** 339–350.

Moutinho, A., Trewavas, A.J., and Malhó, R. (1998). Relocation of a Ca^{2+}-dependent protein kinase activity during pollen tube reorientation. Plant Cell **10:** 1499–1510.

Myers, C., Romanowsky, S.M., Barron, Y.D., Garg, S., Azuse, C.L., Curran, A., Davis, R.M., Hatton, J., Harmon, A.C., and Harper, J.F. (2009). Calcium-dependent protein kinases regulate polarized tip growth in pollen tubes. Plant J. **59:** 528–539.

Nagai, T., Ibata, K., Park, E.S., Kubota, M., Mikoshiba, K., and Miyawaki, A. (2002). A variant of yellow fluorescent protein with fast and efficient maturation for cell-biological applications. Nat. Biotechnol. **20:** 87–90.

Nagai, T., Yamada, S., Tominaga, T., Ichikawa, M., and Miyawaki, A. (2004). Expanded dynamic range of fluorescent indicators for Ca $(^{2+})$ by circularly permuted yellow fluorescent proteins. Proc. Natl. Acad. Sci. USA **101:** 10554–10559.

Negi, J., Matsuda, O., Nagasawa, T., Oba, Y., Takahashi, H., Kawai-Yamada, M., Uchimiya, H., Hashimoto, M., and Iba, K. (2008). CO_2 regulator SLAC1 and its homologues are essential for anion homeostasis in plant cells. Nature **452:** 483–486.

Nour-Eldin, H.H., Hansen, B.G., Nørholm, M.H., Jensen, J.K., and Halkier, B.A. (2006). Advancing uracil-excision based cloning towards an ideal technique for cloning PCR fragments. Nucleic Acids Res. **34:** e122.

Pei, Z.M., Kuchitsu, K., Ward, J.M., Schwarz, M., and Schroeder, J.I. (1997). Differential abscisic acid regulation of guard cell slow anion channels in *Arabidopsis* wild-type and *abi1* and *abi2* mutants. Plant Cell **9:** 409–423.

Pierson, E.S., Miller, D.D., Callaham, D.A., Shipley, A.M., Rivers, B.A., Cresti, M., and Hepler, P.K. (1994). Pollen tube growth is coupled to the extracellular calcium ion flux and the intracellular calcium gradient: Effect of BAPTA-type buffers and hypertonic media. Plant Cell **6:** 1815–1828.

Pierson, E.S., Miller, D.D., Callaham, D.A., van Aken, J., Hackett, G., and Hepler, P.K. (1996). Tip-localized calcium entry fluctuates during pollen tube growth. Dev. Biol. **174:** 160–173.

Pina, C., Pinto, F., Feijó, J.A., and Becker, J.D. (2005). Gene family analysis of the Arabidopsis pollen transcriptome reveals biological implications for cell growth, division control, and gene expression regulation. Plant Physiol. **138:** 744–756.

Qu, H.Y., Shang, Z.L., Zhang, S.L., Liu, L.M., and Wu, J.Y. (2007). Identification of hyperpolarization-activated calcium channels in apical pollen tubes of *Pyrus pyrifolia.* New Phytol. **174:** 524–536.

Roelfsema, M.R.G., and Hedrich, R. (2005). In the light of stomatal opening: New insights into 'the Watergate'. New Phytol. **167:** 665–691.

Roelfsema, M.R.G., Hedrich, R., and Geiger, D. (2012). Anion channels: Master switches of stress responses. Trends Plant Sci. **17:** 221–229.

Russinova, E., Borst, J.-W., Kwaaitaal, M., Caño-Delgado, A., Yin, Y., Chory, J., and de Vries, S.C. (2004). Heterodimerization and endocytosis of *Arabidopsis* brassinosteroid receptors BRI1 and AtSERK3 (BAK1). Plant Cell **16:** 3216–3229.

Sanford, J.C., Smith, F.D., and Russell, J.A. (1993). Optimizing the biolistic process for different biological applications. Methods Enzymol. **217:** 483–509.

Sawano, A., and Miyawaki, A. (2000). Directed evolution of green fluorescent protein by a new versatile PCR strategy for site-directed and semi-random mutagenesis. Nucleic Acids Res. **28:** E78.

Scherzer, S., Maierhofer, T., Al-Rasheid, K.A., Geiger, D., and Hedrich, R. (2012). Multiple calcium-dependent kinases modulate ABA-activated guard cell anion channels. Mol. Plant **5:** 1409–1412.

Schiøtt, M., Romanowsky, S.M., Baekgaard, L., Jakobsen, M.K., Palmgren, M.G., and Harper, J.F. (2004). A plant plasma membrane Ca2+ pump is required for normal pollen tube growth and fertilization. Proc. Natl. Acad. Sci. USA **101:** 9502–9507.

Schmidt, C., Schelle, I., Liao, Y.J., and Schroeder, J.I. (1995). Strong regulation of slow anion channels and abscisic acid signaling in guard cells by phosphorylation and dephosphorylation events. Proc. Natl. Acad. Sci. USA **92:** 9535–9539.

Schroeder, B.C., Cheng, T., Jan, Y.N., and Jan, L.Y. (2008). Expression cloning of TMEM16A as a calcium-activated chloride channel subunit. Cell **134:** 1019–1029.

Schroeder, J.I., and Hagiwara, S. (1989). Cytosolic calcium regulates ion channels in the plasma membrane of *Vicia faba* guard cells. Nature **338:** 427–430.

Schroeder, J.I., Schmidt, C., and Sheaffer, J. (1993). Identification of high-affinity slow anion channel blockers and evidence for stomatal regulation by slow anion channels in guard cells. Plant Cell **5:** 1831–1841.

Shang, Z.L., Ma, L.G., Zhang, H.L., He, R.R., Wang, X.C., Cui, S.J., and Sun, D.Y. (2005). Ca^{2+} influx into lily pollen grains through a hyperpolarization-activated Ca^{2+}-permeable channel which can be regulated by extracellular CaM. Plant Cell Physiol. **46:** 598–608.

Shipley, A.M., and Feijó, J.A. (1999). The use of the vibrating probe technique to study steady extracellular currents during pollen germination and tube growth. In Fertilization in Higher Plants, M. Cresti, G. Cai, and A. Moscatelli, eds (Berlin Heidelberg: Springer-Verlag), pp. 235–252.

Steinhorst, L., and Kudla, J. (2012). Calcium - a central regulator of pollen germination and tube growth. Biochim. Biophys. Acta. **1833:** 1573–1578.

Tavares, B., Dias, P.N., Domingos, P., Moura, T.F., Feijó, J.A., and Bicho, A. (2011a). Calcium-regulated anion channels in the plasma membrane of Lilium longiflorum pollen protoplasts. New Phytol. **192:** 45–60.

Tavares, B., Domingos, P., Dias, P.N., Feijó, J.A., and Bicho, A. (2011b). The essential role of anionic transport in plant cells: The pollen tube as a case study. J. Exp. Bot. **62:** 2273–2298.

Vahisalu, T., Kollist, H., Wang, Y.F., Nishimura, N., Chan, W.Y., Valerio, G., Lamminmäki, A., Brosché, M., Moldau, H., Desikan, R., Schroeder, J.I., and Kangasjärvi, J. (2008). SLAC1 is required for plant guard cell S-type anion channel function in stomatal signalling. Nature **452:** 487–491.

Wang, H.-J., Wan, A.-R., and Jauh, G.-Y. (2008a). An actin-binding protein, LILIM1, mediates calcium and hydrogen regulation of actin dynamics in pollen tubes. Plant Physiol. **147:** 1619–1636.

Wang, Y., Zhang, W.-Z., Song, L.-F., Zou, J.-J., Su, Z., and Wu, W.-H. (2008b). Transcriptome analyses show changes in gene expression to accompany pollen germination and tube growth in Arabidopsis. Plant Physiol. **148:** 1201–1211.

Wang, Y.F., Fan, L.M., Zhang, W.Z., Zhang, W., and Wu, W.H. (2004). Ca^{2+}-permeable channels in the plasma membrane of Arabidopsis pollen are regulated by actin microfilaments. Plant Physiol. **136:** 3892–3904.

Weisenseel, M.H., and Jaffe, L.F. (1977). The major growth current through lily pollen tubes enters as K^+ and leaves as H^+. Planta **133:** 1–7.

Weisenseel, M.H., Nuccitelli, R., and Jaffe, L.F. (1975). Large electrical currents traverse growing pollen tubes. J. Cell Biol. **66:** 556–567.

Winship, L.J., Obermeyer, G., Geitmann, A., and Hepler, P.K. (2010). Under pressure, cell walls set the pace. Trends Plant Sci. **15:** 363–369.

Winship, L.J., Obermeyer, G., Geitmann, A., and Hepler, P.K. (2011). Pollen tubes and the physical world. Trends Plant Sci. **16:** 353–355.

Wu, F.-H., Shen, S.-C., Lee, L.-Y., Lee, S.-H., Chan, M.-T., and Lin, C.-S. (2009). Tape-*Arabidopsis* Sandwich - a simpler *Arabidopsis* protoplast isolation method. Plant Methods **5:** 16.

Wu, Y., Xu, X., Li, S., Liu, T., Ma, L., and Shang, Z. (2007). Heterotrimeric G-protein participation in *Arabidopsis* pollen germination through modulation of a plasmamembrane hyperpolarization-activated Ca^{2+}-permeable channel. New Phytol. **176:** 550–559.

Zhang, H., Qu, X., Bao, C., Khurana, P., Wang, Q., Xie, Y., Zheng, Y., Chen, N., Blanchoin, L., Staiger, C.J., and Huang, S. (2010). *Arabidopsis* VILLIN5, an actin filament bundling and severing protein, is necessary for normal pollen tube growth. Plant Cell **22:** 2749–2767.

Zhao, L.-N., Shen, L.-K., Zhang, W.-Z., Zhang, W., Wang, Y., and Wu, W.-H. (2013). Ca^{2+}-dependent protein kinase11 and 24 modulate the activity of the inward rectifying K^+ channels in *Arabidopsis* pollen tubes. Plant Cell **25:** 649–661.

Zonia, L., and Munnik, T. (2007). Life under pressure: Hydrostatic pressure in cell growth and function. Trends Plant Sci. **12:** 90–97.

Zonia, L., Cordeiro, S., and Feijó, J.A. (2001). Ion dynamics and hydrodynamics in the regulation of pollen tube growth. Sex. Plant Reprod. **14:** 111–116.

Zonia, L., Cordeiro, S., Tupý, J., and Feijó, J.A. (2002). Oscillatory chloride efflux at the pollen tube apex has a role in growth and cell volume regulation and is targeted by inositol 3,4,5,6-tetrakisphosphate. Plant Cell **14:** 2233–2249.